Recombinant VEGF-C restores mesenteric lymphatic drainage and improves gut immune surveillance in experimental cirrhosis

Pinky Juneja[1]#, Syed Nazrin Ruhina Rahman[2]#, Dinesh M Tripathi[1], Impreet Kaur[1], Sumati Rohilla[1], Abhishek Gupta[1], Preety Rawal[1], Sukriti Baweja[1], Archana Rastogi[3], VGM Naidu[4], Shiv K Sarin[5], Subham Banerjee[2*], Savneet Kaur[1*]

[1]Department of Molecular and Cellular Medicine, Institute of Liver and Biliary Sciences, New Delhi
[2]Department of Pharmaceutics, National Institute of Pharmaceutical Education and Research (NIPER)-Guwahati, Changsari, Assam, India.
[3]Department of Pathology, Institute of Liver and Biliary Sciences, New Delhi
[4]Department of Pharmacology and Toxicology, NIPER-Guwahati, Changsari, Assam, India.
[5]Department of Hepatology, Institute of Liver and Biliary Sciences, New Delhi

#Shared first author
[*]Corresponding author

[*]Correspondence

Dr. Savneet Kaur, Assistant Professor, Department of Molecular and Cellular Medicine, Institute of Liver and Biliary Sciences, New Delhi, India, Phone no. 91-11-46300000,
E-mail: savykaur@gmail.com

Dr. Subham Banerjee, Associate Professor, Department of Pharmaceutics, NIPER-Guwahati, Changsari-781125, Assam, India. E-mail: subham.banerjee@niperguwahati.ac.in

All authors declare no competing interest

Abstract

Gut lymphatic vessels (LVs) are crucial for maintaining immunity and abdominal fluid homeostasis. In experimental liver cirrhosis with ascites, gut LVs are dilated and dysfunctional with impaired gut immune response. Therapy with pro-lymphangiogenic factor, vascular endothelial growth factor-C (VEGF-C), promotes functional LVs growth and attenuates inflammation. However, therapeutic role of VEGF-C in cirrhosis has not been explored. Here we developed a nanoformulation comprising VEGF-C-loaded reverse-micelles (E-VEGF-C) and delivered orally in rat models of liver cirrhosis to specifically target mesenteric LVs (mLVs). E-VEGF-C treated cirrhotic rats displayed increased density of mLVs, improved functional drainage, and reduced abdominal fluid/ascites and portal pressures without any adverse events. E-VEGF-C also enhanced the proliferation of LVs in mesenteric lymph nodes triggering active immune responses, which helped to contain spreading of bacteria to other organs preventing systemic infection. Collectively, E-VEGF-C in cirrhotic rats ameliorates drainage of mLVs, ascites formation, and immunity; thus, represents potential treatment to manage ascites and immune dysfunction in cirrhosis.

Keywords: Cirrhosis; Gut Lymphatic vessels; Lymphangiogenesis; Portal Hypertension; Targeted nanodelivery

Introduction

Chronic liver disease is associated with significant morbidity and mortality worldwide [1,2]. They can progress from mild fibrosis to cirrhosis, which may further progress to end-stage liver disease with the onset of decompensation such as ascites, hepatic encephalopathy and, variceal bleeding[3]. In addition to other underlying factors, a deranged gut-liver axis plays a significant role in the progression of liver disease[4,5]. Whatever comes from the gut, enters the liver through portal circulation before returning to the heart and systemic blood via the hepatic vein. However lymphatic channels in the gut bypass the portal circulation in the liver and directly connect the gut to the systemic circulation via the thoracic duct[6].

Gut lymphatic vessels (LVs) plays essential roles in the absorption and transportation of fat, maintenance of fluid homeostasis, removal of interstitial fluid, macromolecules, immune cells, and microbial debris from the intestine, and returning lymph to the blood circulation, thereby preventing edema and abdominal ascites[7]. Lymphangiogenesis in the gut during inflammation compensates for lymphatic insufficiency in patients with inflammatory bowel disease (IBD), such as Crohn's disease, where there is both an increase and a redistribution of lymphatic vessels[8,9]. In liver cirrhosis, the production of abdominal lymph increases 30-fold, and there is a positive correlation between lymph flow and increasing portal pressure[10,11]. Using animal models of CCl4-induced liver damage, an elegant study reported that gut LVs show an impaired phenotype and reduced contractility in cirrhosis[12].

Vascular endothelial growth factor-C (VEGF-C), a key pro-lymphangiogenic factor, primarily activates lymphangiogenesis by binding to tyrosine kinase receptor, VEGFR3, and the downstream Akt/Erk pathway[13]. Therapies aimed at enhancing lymphangiogenesis and improving lymphatic transport and function with VEGF-C have been shown to be effective for improving lymphatic drainage and ameliorating inflammation in diseases such as IBD, rheumatoid arthritis, skin inflammation, and hepatic encephalopathy[14–17]. The short half-life and systemic side effects of these growth factors are however some of the major hurdles that limit their clinical application[18].

Here, we hypothesized therapeutic role of VEGF-C for the restoration of gut lymphatic drainage and immune response in cirrhosis. VEGF-C, a hydrophilic molecule, carries positive charge at physiological pH with short half-life and is highly unstable in nature[19,20]. To minimize the side effects of systemic delivery and increase the gut bioavailability of VEGF-C, we fabricated an engineered VEGF-C protein using human recombinant VEGF-C protein (Cys156Ser), encapsulated it within nanoscale reverse micelle based lipo-carriers and delivered it via oral route to ensure lymphatic uptake for targeted gut lymphangiogenesis in vivo.

Results

Mesenteric Lymphatic Vessel proliferation or lymphangiogenesis is increased in experimental cirrhosis

To first evaluate mesenteric LVs (mLVs) in liver cirrhosis, we performed immunohistochemical staining of mesentery sections in control rats and experimental models of liver cirrhosis with antibodies recognizing Podoplanin (Pdpn), a widely accepted marker of lymphatic vasculature. Control rats showed sporadic, thin LVs in the vicinity of blood vessels, whereas cirrhotic rat mesentery tissues contained numerous, readily detectable, and dilated LVs compared to control (**Figure 1A-C**). Quantitative analysis of the same section revealed that the total number of Pdpn+ LVs per field in CCl4 rat specimens was significantly higher with increased diameter compared to control (**Figure 1B, C** $p<0.05$). The mRNA level of LVs markers, Prox1 (5-fold change) and LyVE1 (18-fold change), were also enhanced in the mesentery of cirrhotic rats compared to the control (**Figure 1D**, $p<0.05$). Also, CCL21, COX2, and eNOS mRNA level was upregulated, reflecting an inflamed gut. VEGF-C expression was upregulated in CCl4 rat mesentery (although not significant), suggesting inflammation-induced lymphangiogenesis ($p>0.05$,

Figure 1D). VEGF-C/VEGFR3 axis is pronounced in intestinal lymphangiogenesis and inflammation-induced lymphangiogenesis[16]. Therefore, we checked the expression of VEGFR3 by immunofluorescence staining in mesentery sections of control and CCL4 rats. The protein expression of VEGFR3 was significantly increased in the cirrhotic animals compared to that seen in the control (**Figure 1E, F** $p<0.01$). Collectively, these data demonstrate that the number of mLVs increases in liver cirrhosis.

Development of Nanoengineered E-VEGF-C for targeted delivery to Gut Lymphatic Vessels

Given the fact that there exists a dilation and lymph transport failure of the mLVs in experimental cirrhosis with ascites[12], we hypothesized that enhancing the number of new functional LVs in the mesentery by treatment with lymphangiogenic factors, VEGF-C, may improve lymphatic drainage in cirrhotic rats. To this end, we developed an engineered VEGF-C (E-VEGF-C) in a nanoformulation to enhance LV uptake in the intestine after oral delivery (**Supp Figure 1**). Human recombinant VEGF-C protein (rhVEGF-C- Cys156Ser), which specifically binds to the VEGFR3 homodimer present on lymphatic endothelial cells (LyECs), was encapsulated inside the lipocarriers prepared with distearoyl-rac-glycerol-PEG2K (**Figure 2A**). In dynamic light scattering (DLS) analysis, the z-average/mean particle size (MPS) of E-VEGF-C was found to be 134.8 ± 0.47 nm with a polydispersity index (PDI) value of 0.126 ± 0.01 (**Figure 2B**). The zeta potential (ZP) value of the E-VEGF-C was -21.9 ± 1.24 mV (**Figure 2C**). The pH of the E-VEGF-C nanoformulation was 6.369 Â ± 0.004. Stability study up to one month indicated no drastic change in the physicochemical properties (MPS, PDI, and ZP values) of the E-VEGF-C nanoformulation **(Supp Table 1).** The surface morphology and size of E-VEGF-C were studied using field emission-scanning electron microscope (FE-SEM), and field emission-transmission electron microscopy (FE-TEM) indicated that the particles were spherical and smooth in appearance and uniformly distributed (**Figure 2D, E**). Atomic force microscopy (AFM) micrographs provided two-dimensional (2D) and three-dimensional (3D) images of the E-VEGF-C surface morphology and showed that E-VEGF-C was compact, smooth, and spherical in shape (**Figure 2F**). The average diameter of individual particles in the prepared reverse micelles (RM) was 16 nm. The encapsulation efficiency of VEGF-C-loaded RMs was 93.28 ± 1.85 %. The release profile of VEGF-C-loaded RMs was performed in PBS at pH 7.4, which showed an initial burst release of 31.95 ± 1.52 % VEGF-C-loaded RMs was observed at 2 hr post mixing, followed by an increase in VEGF-C release of 84.66 ± 1.82 % at 4 hrs. which then gradually decreased at other post-mixing time points (**Figure 2G).** After the *in vitro* release study, the obtained data were fitted to different kinetic models. The R^2 values obtained from the different kinetic models are listed in **Supp Table 2,** which suggests that the VEGF-C release from RMs showed zero order release and, therefore, independent of concentration.

In vitro and in vivo Bio-distribution of E-VEGF-C

To investigate the internalization of E-VEGF-C *in vitro*, we isolated and sorted Pdpn and CD31 positive LyECs from rat mesenteric tissue and mesenteric lymph nodes (MLN) using fluorescence-activated cell sorting (FACS) (**Supp Figure 2A, B**) and incubated with coumarin-6-labelled E-VEGF-C. Fluorescence microscopy revealed the efficient internalization of E-VEGF-C by LyECs at 4hrs. (**Figure 3A, B**). Next, to ensure the specificity of E-VEGF-C delivery *in vivo*, tissue biodistribution studies of coumarin-tagged E-VEGF-C were performed two hours post its oral administration using spectrofluorimetry and fluorescence microscopy **(Figure 3C).** A weak fluorescence signal was observed in almost all tissues in both the control and CCl4 rats (**Supp Figure 2C**). In comparison, an intense fluorescence signal was observed in the mesentery of control and cirrhotic rats (**Figure 3D, E**). CCl4 cirrhotic rats also showed increased human VEGF-C levels in the mesenteric and duodenal tissues compared to control rats(**Figure 3F,** $P< 0.05$). In the serum of CCl4 animals, levels of VEGF-C exhibited a biphasic peak; the first peak appeared at about 10 min, and the second peak appeared at approximately 5 hrs. (**Figure 3G**). There were no adverse effects or mortality after E-VEGF-C treatment in either control or CCl4 rats.

E-VEGF-C treatment induces Mesenteric Lymphatic Vessel proliferation

Next, we studied the therapeutic effects of E-VEGF-C in animal models of liver cirrhosis. Rats were intraperitoneally injected with CCl4 for 12 weeks or till ascites formation. One week after ascites formation, 600µg/kg of E-VEGF-C was administered orally on consecutive days for up to 2 weeks (**Figure 4A**). The animals were sacrificed at 48 hrs. after the last dose of E-VEGF-C. Immunohistochemical analysis of the mesentery showed increased numbers of Pdpn+ mLVs with reduced diameter in E-VEGF-C rats compared to CCl4-V cirrhotic rats ($p<0.05$, **Figure 4B-D**). Along with this, significantly increased lymphangiogenesis is observed in MLNs of E-VEGF-C rats compared to CCl4-V and control rats ($p<0.05$, **Figure 4E, F**). Mesenteric tissues also revealed a reduction in the inflammation in the E-VEGF-C rats compared to that seen in CCl4-V rats, which correlated with a reduction in mRNA expression of the inflammatory markers eNOS and iNOS after E-VEGF-C treatment (**Supp Figure 3A, B**). Next, we analyzed the protein expression of human VEGF-C in the mesentery tissues of different study groups. Results demonstrated a significant increase in human VEGF-C protein in the mesentery with MLN tissue extracts of E-VEGF-C-treated rats compared to the vehicle ($p<0.01$, **Figure 4G, H**). Since VEGF-C also participates in blood vessel angiogenesis in some tissues, we also evaluated whether E-VEGF-C had any effects on blood vessels in mesentery . We observed no significant difference in the number of CD31-positive vessels between the CCl4-V and E-VEGF-C rats ($p>0.05$, **Supp Figure 3C, D**).

E-VEGF-C treatment Improves Drainage of Mesenteric Lymphatic Vessels

To investigate the effect of E-EVGFC on LVs patterning, whole-mount immunostaining of the mesenteric tissues was performed in all study groups using pdpn antibody. In control rats, thin LVs of diameter ranging from 50 to 80 µm were observed, which were increased to 100 to 150 µm in CCl4-V rats. In E-VEGF-C treated rats, sprouting of new LVs from the existing one was clearly observed with reduced diameter ranging from 60 to 100 µm compared to the CCl4-V rats (**Figure 5A, B**). Branching points of mLVs close to the intestine were also increased in the E-VEGF-C rats in comparison to CCL4-V (**Figure 5C**, **D**). To assess the functionality of LVs, we gavaged the rats with BODIPY FL-C16 and analyzed the drainage and leakage of mLVs after 2hrs using confocal micrscopy. (**Figure 5E).** CCl4 rats displayed increased BODIPY fluorescence inside mLVs with an increased diameter compared to the control rat's mLVs, which represents the accumulation of dye and, hence, incomplete drainage. On the other hand, E-VEGF-C-treated rats had significantly reduced fluorescence inside the mLVs with decreased diameter ($p<0.001$, **Figure 5F-H**). Dilated LVs cause leakage of the lymph and accumulation in tissue spaces, leading to inflammation. To assess leakage from the LVs, fluorescence just outside the mLVs was quantified. We observed increased fluorescence outside the LVs in CCl4 rats compared to control rats, which was significantly reduced in E-VEGF-C rats ($p<0.001$, **Figure 5I**).

E-VEGF-C reduces Ascites and ameliorates Portal Pressure in Cirrhotic and Non-cirrhotic Portal Hypertensive Rats

We next probed whether an improvement in lymphatic drainage, with proliferation of mLVs , and decrease in mesenteric inflammation in E-VEGF-C treated rats had any effect on ascitic fluid volume. CT scan analysis of all study groups was performed to observe the ascites in the peritoneal cavity. No ascites was observed in the control group, whereas all CCl4-V cirrhotic rats displayed severe ascites **(Figure 6A).** At the end of E-VEGF-Ctreatment, we assessed the volume of peritoneal fluid. E-VEGF-C rats displayed a marked reduction in ascites volume as compared to that observed in CCl4-V rats, as was also clearly evident in CT scan slices of the two groups ($P< 0.001$, **Figure 6A, B, Supp Table 3**). Along with ascites reduction, Evans blue staining showed a significant increase in plasma volume in the E-VEGF-C group compared with the vehicle group ($P< 0.05$, **Figure 6C**).

Next, we analyzed whether this reduction in ascitic fluid volume after E-VEGF-C treatment was also associated with liver physiology and pathological changes. Intraperitoneal CCl4 treatment for 12 weeks markedly increased portal pressure (PP) in rats compared to that in control rats ($p<0.001$, **Figure 6D**). However, E-VEGF-C treatment significantly attenuated PP compared to vehicle rats ($p<0.001$, **Figure 6D**). To ascertain whether the observed reduction in PP was due to a change in the portal blood flow (PBF) or intrahepatic resistance (IHR), we also monitored these parameters in all study groups. E-VEGF-C treatment significantly decreased PBF, in turn increasing the mean arterial pressure (MAP) as compared to that of the CCl4-V rats ($p<0.05$, **Figure 6D, Supp Figure 4**). However, IHR in E-VEGF-C-treated rats was similar to that in cirrhotic rats ($p>0.05$, **Figure 6D**). Compared to control rats, liver weights in E-VEGF-C and CCl4-V rats were also similar (**Supp Figure 4**). We next evaluated changes in the histological and biochemical parameters of the liver in cirrhotic animals. Masson's trichrome staining of liver tissues revealed that both CCl4-V and E-VEGF-C rats showed Ishak fibrosis scores of 5/6 or 6/6, indicating complete cirrhosis (thick fibrous septa or many minute nodules) (**Figure 6E**). Regarding biochemical parameters, CCl4 treatment resulted in a significant increase in serum ALT levels and decreased albumin levels compared to those in the control group (**Supp Table 3**). There was no significant improvement in serum albumin and ALT levels in E-VEGF-C-treated rats compared to CCl4 rats. The kidney function test results were normal in all study groups (**Supp Table 3**).

We also investigated whether E-VEGF-C treatment improved PP irrespective of liver cirrhosis by measuring hepatic hemodynamics in non-cirrhotic portal hypertensive (PPVL) animals (**Supp Figure 7A**). Histology of these animals displayed portal inflammation in the liver but no significant fibrosis (**Supp Figure 5A, B**). In the mesentery of E-VEGF-C-treated PPVL rats showed an increased presence of VEGFR3+ LVs and reduced inflammation compared to PPVL vehicle animals (**Supp Figure 5C, D**). PPVL animals treated with E-VEGF-C also displayed increased human VEGF-C protein expression compared to vehicle rats (**Supp Figure 5E, F**). Hemodynamic analysis revealed a significant reduction in the PP and PBF of PPVL animals treated with E-VEGF-C compared with vehicle animals ($p< 0.01$, **Figure 6F**). The expression of bFGF, CCL21, iNOS, and eNOS was significantly higher in the mesentery of PPVL vehicle animals than in controls. In E-VEGF-C-treated PPVL rats, there was a significant reduction in iNOS and eNOS levels compared to the vehicle group, whereas bFGF increased. ($p<0.05$, **Supp Figure 5G**).

E-VEGF-C treatment modulates gene expression in lymphatic endothelial cells (LyECs) of mesentery

To gain mechanistic insights into VEGF-C-induced lymphangiogenesis in mLVs, LyECs from mesentery and MLNs were isolated using FACS and the expression of relevant genes was examined. (**Figure 7A**). The mRNA level of differentiation and proliferation markers of LyECs, i.e., Prox1 and LyVE1, , were upregulated in LyECs of E-VEGF-C treated rats compared to vehicle. ($p<0.05$, **Figure 7B**). Collecting LVs generally present in mesentery, prevents any leakage of lymph by zippering between LyECs using VE-cadherin and VCAM-1. mRNA levels of VCAM1 decreases in LyECs of CCL4-V rats, indicating leaky mLVs causing more inflammation. No significant change is observed in VE-cadherin in CCl4-V rats compared to control. Treatment with E-VEGF-C led to increased expression of both VCAM1 and VE-cadherin in LyECs correlating with decreased leakage of lymph from mLVs. ($p<0.05$). LyECs also act as APCs, present Ag to T cells for tolerance or induction of immune response. The costimulatory marker, CD86, was also significantly upregulated in LyECs of treated rats . In contrast, no significant change was observed in MHC II levels in the vehicle vs. treated group ($p>0.05$). The inflammatory marker COX2 was markedly increased in LyECs of CCl4-V rats suggesting inflamed lymphatic endothelium, which further reduced in the LyECs of treated group ($p<0.05$). CCL21 chemokine mRNA level is found to be increased in LyECs of both CCl4-V and E-VEGF-C treated rats compared to control ($p<0.05$).

E-VEGF-C increases the trafficking of immune cells and clearance of bacteria load in mesenteric lymph node

LyECs secrete chemokines, interact with immune cells, primarily T cells and dendritic cells (DCs), and present antigens to generate an immune response against invading pathogens. VEGF-C also increases immune cell trafficking to the lymph nodes[17,21]. Therefore, to study the effect of E-VEGF-C treatment on immune cell trafficking to MLNs, cells were isolated from MLN of all study groups and labeled with antibodies for T cell subsets and DCs for quantification using flow cytometry (**Supp Figure 6A, B**). The total T cell, Th and Tc cell population in MLNs did not change significantly in control and CCl4-V as previously reported[22]. Treatment with E-VEGF-C also led to no change in the above-mentioned population. We further quantified recently activated T cell with CD134 and regulatory T cell with CD25 expression. No significant change was observed in CD134 expression in varied groups (**Figure 8A, B)** but we observe a significant decrease in CD8 Treg cells after E-VEGF-C treatment in comparison to CCl4-V (**Figure 8C-D**). DCs, along with the expression of T cell activation coreceptor CD80, were increased after treatment with E-VEGF-C compared to that observed in the vehicle ($p<0.05$, **Figure 8E**).
Gut immune response is dysfunctional in cirrhosis, leading to spread of PAMPs and DAMPs, causing infection and inflammation. Though we observed no significant changes in T cell subsets in MLNs of either CCl4-V or E-VEGF-C, we wanted to look for any change in immune response in the presence of antigen challenge, therefore , we performed a few experiments with live bacteria[23]. To analyze the effect of activated T cells and DCs on bacterial clearance in MLNs after E-VEGF-C treatment, we gavaged the rats with GFP-labelled *Salmonella typhimurium* in large numbers in all study groups (**Figure 8F**). MLNs, liver, spleen, lung, and blood were collected after 48 hrs. of incubation. In control rats, GFP-labelled bacteria were found only in the MLNs, whereas in CCl4-V, GFP-labelled bacterial load was present in almost all tissue collected, including the blood (**Figure 8G**, **Supp Figure 6C**). Interestingly, in E-VEGF-C treated rats, bacterial translocation was confined only to the MLNs with reduced live bacteria than CCl4-V (**Figure 8G, H**), suggesting clearance of bacterial load. We also quantified the T cell subsets in MLNs and found a significant increase in recently activated Th cells in MLNs of E-VEGF-C treated rats compared to CCl4-V, which indicate active immune response in MLNs in the presence of antigen (**Figure 8I-L**).

Decrease in endotoxins after E-VEGF-C administration in liver cirrhosis

Since immune response is found be increased in MLNs of E-VEGF-C treated rats after live bacteria challenge, , we next studied whether the treatment also affected systemic inflammation. We assessed the levels of TNF-α and endotoxins in the ascitic fluid and serum. Serum endotoxin and TNF-α levels were considerably higher in CCl4-V rats than in control rats ($p<0.01$; **Figure 9A, B**). We did not observe any significant changes in the serum endotoxin, and TNF-α levels in the E-VEGF-C treated rats compared to CCl4-V rats. In the ascitic fluid, there was, however, a significant decrease in the levels of endotoxins per milliliter in the treated rats compared to the CCl4-V cirrhotic rats ($p<0.05$, **Figure 9C, D**) though no change is observed in TNF-α levels in CCl4-V and E-VEGF-C treated rats.

Discussion

In this study, we investigated morphological and molecular alterations of mLVs and MLNs in experimental cirrhosis and portal hypertension. We report significantly increased number of dilated pdpn+ and VEGFR3+ leaky mLVs with reduced drainage capacity and enhanced inflammatory markers in cirrhotic and portal hypertensive animals clearly implying gut lymphatic dysfunction similar to that observed in intestinal lymphangiectasia and gut inflammatory disorders[24,25]. An increase in mLVs density in cirrhosis may be attributed to a compensatory lymphangiogenesis response to lymphatic occlusion[26]. A previous study in cirrhotic rats documented that an increased expression of eNOS in the mesenteric LyECs was the cause of dysfunctional and dilated lymphatics in cirrhosis and that inhibiting eNOS

improved the lymphatic transport of the existing vessels by increasing the contractile activity of these vessels[12]. In our study, instead of manipulating the contractile activity of the existing mLVs using an eNOS inhibitor, we focused on increasing the number of new functional lymphatic channels via VEGF-C treatment.

Given the short half-life and systemic effects of VEGF-C[18], we constructed a therapeutic recombinant VEGF-C molecule using RM-based nanolipocarriers. RM nanolipocarriers are nanoparticle-sized water-in-oil microemulsions with controlled particle sizes. A recent report illustrated the therapeutic potential of the fully human fusion protein F8-VEGF-C (VEGF-C linked to F8 antibody) for targeted delivery of VEGF-C in mouse models of chronic inflammatory skin disease[27]. However, the study did not report sustained release of VEGF-C. In another study, VEGF-C mRNA was encapsulated in lipid nanoparticles for the sustained release at administration site and found to be effective in treating experimental lymphedema[28]. We used various strategies in this study to ensure a targeted and sustained delivery of VEGF-C in the mLVs. First, the use of RM-based lipid nanocarriers allowed the VEGF-C cargo to be carried in the chylomicron-sized particles in the LVsafter oral delivery. Encapsulation also ensured their sustained and programmable release[29]. The *in vitro* uptake assay clearly showed more than 90% uptake of the E-VEGF-C by LyECs isolated from mesentery. The *in vitro* release studies indicated a more than 80% VEGF-C release in about 4 hrs. and *in vivo* the release profile showed a biphasic peak, with the initial burst coming at approximately 10 min, and the second peak at about 5 h. Biphasic drug release is a characteristic feature of drugs encapsulated in nanolipocarriers[30]. In the *in vivo* biodistribution studies as well, cirrhotic rats had maximum levels of E-VEGF-C in the mesenteric tissues, indicating the efficacy of our delivery vehicle. We did not follow any conjugation chemistry for the preparation of the E-VEGF-C molecule, rather, we focused on the preparation of simple solid lipid nanoparticles with an aqueous template using a modified multiple emulsification technique, as previously reported[31].

Treatment with E-VEGF-C markedly enhanced the expression of VEGF-C protein in the mesentery, along with a concomitant increase in the sprouting of pdpn+ and VEGFR3+ LVsboth in the mesentery and the MLNs, suggestive of a VEGF-C driven proliferation of LyECs[32]. The dilations observed in the mLVs of cirrhotic animals were also attenuated with E-VEGF-C treatment[33]. Specific genes, such as Prox1 and LyVE1, were significantly increased in the mesenteric LyECs of E-VEGF-C rats, indicating pronounced differentiation and proliferation of LyECs. Expression of inflammatory genes, such as Cox2, was decreased, while VCAM-1 and VE-cadherin, which govern cell adhesion and vessel permeability, increased in E-VEGF-C rats. The functional implications of enhanced gene expression were evident in terms of reduced inflammation, lymph leakage and improved drainage in E-VEGF-C treated rats. This is in accordance with many previous studies showing the drainage-promoting function of VEGF-C in experimental models of bacterial skin inflammation and inflammatory bowel disease[34,35]. An improvement in lymphatic drainage and functionality of the mLVsin cirrhotic rats was also associated with a marked reduction in ascitic fluid volume in rats with fully developed ascites. A decrease in ascites was accompanied by an increase in the plasma volume of treated rats, suggesting that ascites may have been reabsorbed into the circulating blood[11].

Along with a reduction in ascites, there was also a significant decrease in PP in cirrhotic portal hypertensive rats treated with E-VEGF-C, which was associated with attenuated PBF and increased MAP. However, there was no change in IHR, indicating that improvement in PBF and not hepatic resistance (fibrosis) led to an improvement in portal pressure after treatment. A decrease in PP may be caused by a reduction in intra-abdominal pressure that may have occurred during the drainage of ascitic fluid into newly formed mLVs. It has been postulated that the removal of ascites plays a role in postparacentesis systemic hemodynamic changes through mechanical decompression of the splanchnic vascular bed[36]. However, a reduction in PP due to an increase in the number of LVsand a decrease in interstitial fluid pressure may also have led to a decrease in ascites[11]. Intriguingly, this decrease in PP and ascites was also observed in the non-cirrhotic PPVL animals after E-VEGF-C treatment, validating the favorable effects of

pro-lymphangiogenic treatment on PBF and systemic hemodynamics. An improvement in PP was not associated with a significant improvement in liver pathology in the treated rats, indicating that there were no protective effects of E-VEGF-C treatment on the hepatic compartment per se. We also did not observe any major changes in the serum albumin or ALT levels in the treated animals. In our study, we administered therapeutic E-VEGF-C treatment in decompensated animal models when liver cirrhosis and ascites had already been established. It would be worthwhile to evaluate the effects of E-VEGF-C on the early onset of decompensation and liver pathology in compensated cirrhotic models of portal hypertension using a preventive treatment approach.

Mesenteric angiogenesis, marked by an increase in CD31+ vessels, is a common feature of cirrhosis and has also been observed in cirrhotic rats[37]. However, we did not detect any significant changes in the density of CD31+ blood vessels in E-VEGF-C-treated cirrhotic rats, indicating that E-VEGF-C did not affect the mesenteric blood vessels, analogous to that previously documented[34,35]. With respect to inflammation, there was a conspicuous decrease in mesenteric tissue inflammation in the E-VEGF-C-treated rats.

VEGF-C is known to increase immune cell trafficking to the draining lymph node[14]. We did not observed any T cell recruitment in the MLNs of E-VEGF-C treated animals. On the other hand, increased in costimulatory markers, CD86, in the LyECs of E-VEGF-C treatmed rats, suggesting active antigen presentation.[38]. MLNs are sentinels of gut immunity that act as barriers to prevent the spread of PAMPs and live bacteria to system and therefore preventing unwanted systemic inflammatory response[39]. In cirrhosis, studies have reported an increased live bacterial translocation to MLNs, causing systemic spread of the infection and therefore multiple organ failure due to sepsis and septic shock[40,41]. In our study, we observed similar results after challenging cirrhotic animals with live bacteria. Along with positive MLNs cultures in cirrhotic rats, we observed live bacteria in other organs and systemic blood as well ascribed to an impaired gut immune response which failed to contain the bacteria into the MLNs. In cirrhotic animals treated with E-VEGF-C, bacteria remained confined to the MLNs only, with a significant increase in recently activated CD4 T cells, suggesting an appropriate immune response in MLNs of treated animals. An earlier study documented that the stimulation of cardiac lymphangiogenesis with VEGF-C improved the trafficking of immune cells to the draining lymph nodes after myocardial infarction resolving inflammation[42]. Along with an improvement of local gut immune response , we also observed a decrease in endotoxins, suggesting attenuation of inflammation after E-VEGF-C treatment[43]. We also observed a reduction in the systemic levels of TNF-α; however, this decrease was not significant, possibly because we administered only a short-term therapeutic E-VEGF-C treatment to the animals after decompensated cirrhosis had completely set-in.

In summary, our study underscores the use of an RM incorporating hydrophilic VEGF-C as a novel therapy for enhancing mesenteric lymphangiogenesis and improving lymphatic drainage and gut immunity by providing an efficient exit route for ascitic fluid, further strengthening the concept of the gut-liver axis. The study proposes E-VEGF-C in a novel nanoengineered format as an innovative and targeted strategy for the management of ascites and portal hypertension in patients with decompensated cirrhosis. Gut LVs-targeted delivery of E-VEGF-C may also open new avenues for the prevention of decompensation in cirrhosis.

Methods

Preparation and Characterization of Engineered VEGF-C

Preparation and characterization of reverse micelles (RMs)

A high-pressure homogenization/microfluidization technique previously reported by Bai *et al. (2019)* was followed with a slight modification for the preparation of RMs. To prepare RMs, Distearoyl-rac-glycerol-PEG2K (DSG-PEG 2000) and Span 80 were dissolved in an organic solvent (ethanol). Span 80 was used as the emulsifier. Double-distilled water containing VEGF-C was added dropwise to the organic phase and mixed well with a digital magnetic stirrer (IKA®-Werke GmbH & Co. KG, Stäüfen, Germany). The coarse dispersion was then passed through a benchtop high-shear homogenizer (LM20, Microfluidics, Massachusetts, USA) at 20,000 pressure for three cycles to obtain nanosized translucent RMs (Supp Figure 1).

Mean particle size (MPS), polydispersity index (PDI) and zeta potential

The MPS, PDI, and ZP values were evaluated using dynamic light scattering (DLS). One hundred microliters of RM sample were diluted with double distilled water up to 1 ml, in triplicate. Using a Malvern Zetasizer (Nano ZS, Malvern Instrument Ltd, Malvern, UK), the MPS, PDI, and ZP values of the diluted RMs were determined at 25 °C by placing 1 ml of sample directly into a standard quartz cuvette. A He-Ne light source at 633-nm wavelength was used as the source of the laser beam in this instrument.

Stability study

the RM formulation was observed over a period of one month at 4°C for the stability study. Samples were withdrawn at regular time intervals of 0, 1, 2, 3, and 4 weeks to observe the influence of storage conditions on MPS, PDI, and ZP values.

pH measurement

The pH of the RM formulation was measured in triplicate using a pH meter (Mettler Toledo, Greifensee, Switzerland) at room temperature.

Field emission-scanning electron microscope (FE-SEM)

The surface morphology and size of the RM formulations were examined using FE-SEM (GeminiSEM 500, Carl Zeiss Microscopy, GmbH, Oberkochen, Germany). Before loading the sample into the FE-SEM

instrument, it was coated with gold to avoid or minimize the charging effect. Images were recorded at a voltage–2-4 kV using an in-lens detector [44].

Atomic force microscopy (AFM)

AFM (Innova SPM, Bruker, Germany) analysis was performed in the non-contact tapping mode to record the topographical images of the optimized RM formulation. The samples were prepared using the drop-casting method, followed by drying at room temperature. The raw data obtained from the system were processed using Gwyddion software, version 2.60.

Field emission-transmission electron microscopy (FE-TEM)

The morphologies and sizes of the RMs were examined using FE-TEM (JEOL, 2100F, Japan). Approximately 10 µl of the sample was dropped onto a carbon-coated copper grid and covered with collodion carbon, followed by air-drying at room temperature before measurements were taken. Images were recorded at an accelerating voltage of 90 kV, and images were recorded.

Determination of encapsulation efficiency (EE %)

The percentage of VEGF-C encapsulated in the formulation was quantified by enzyme-linked immunosorbent assay (ELISA) using the Quantikine™ human VEGF-C ELISA kit protocol [45]. The prepared reverse micelles were placed in a rotary evaporator (IKA®, Werke GmbH & Co. KG, Stäüfen, Germany) to remove the solvent present in the formulation at 58º C temperature, 100 rpm, and -700 to -800 mbar pressure. The thin film obtained was hydrated using double-distilled water. One milliliter of the redispersed formulation was taken and 1 ml of ethanol was added to disrupt the self-assembled structure of the lipid layer. The samples collected in triplicate were analyzed using an ELISA kit at 450 nm with a multimode reader (SpectraMax®, CA, USA) according to the manufacturer's instructions. The EE % was calculated using Equation (1).

$$\text{EE}\,\% = \frac{\text{Amount of } VEGF - C \text{ in formulation}}{\text{Actual amount of } VEGF - C \text{added in formulation}} \times 100 \ldots. \text{Eq. (1)}$$

In vitro VEGF-C release from reverse micelles

The *in vitro* VEGF-C release from the RMs was analyzed by ELISA using the Quantikine™ human VEGF-C ELISA kit protocol [46]. Two milliliters of reverse micelle dispersions containing 666.6 ng VEGF-C were placed in the middle of the dialysis bag. The dialysis bag containing the dispersions was then kept in 5 ml of release medium (phosphate buffer saline, PBS, pH 7.4) in a 50 ml falcon tube. The Falcon tube was then placed in an incubator shaker (REMI Sales & Engineering Ltd., Mumbai, India) at 37 °C with shaking at 75 rpm. The samples were withdrawn at different time points (1, 2, 4, 6, 8, 10, and 24 h), and pre-warmed fresh medium was added at each time point. The collected samples were stored at -20 °C for later analysis. The collected samples were analyzed according to the manufacturer's instructions in the ELISA kit booklet using an ELISA kit at 450 nm with a multimode reader (SpectraMax®, CA, USA). The results are expressed as percent cumulative release ± standard deviation (SD) in triplicate.
The percent cumulative release data were fitted into different release kinetic models, such as zero-order, first-order, Korsmeyer-Peppas, Weibull, Higuchi, and Hixson-Crowell models, using KinetDS software, version 3.0. The best-fit plot was chosen based on the maximum R^2 (coefficient of determination) value [47].

***In vivo* studies**

Study Groups and treatment

All animals received humane care according to the criteria outlined in the ‘‘Guide for the Care and Use of Laboratory Animals’’ prepared by the National Academy of Sciences and published by the National Institutes of Health (NIH publication 86-23 revised 1985). The study was approved by the Animal Ethics Committee of ILBS, New Delhi, according to standard guidelines (Ethics Protocol No: IAEC/ILBS/18/01). Rats were housed in a room at 22 ± 3^0C a 12 hrs. light-dark cycle and were given food and water ad libitum. Studies were performed on thirty-six 8-week-old male Wistar rats and twelve male 8–10-week-old Sprague Dawley (SD) rats weighing 250–300 g. Wistar rats were used to develop cirrhotic models of portal hypertension, while SD rats were utilized for the development of non-cirrhotic portal hypertension models by partial portal vein ligation (PPVL). Animals were randomized into three groups for the cirrhosis study: healthy control group (treated with saline), CCl4-V or vehicle group (CCl4 plus lipid nanocarriers alone without VEGF-C), and E-VEGF-C group (CCl4 plus E-VEGF-C). Cirrhosis was induced by intraperitoneal injection of 1.0 ml/kg body weight of CCl4:olive oil in 1:1 ratio, two times a week for 12-14 weeks until ascites formation. The control group (control) received olive oil 1.0 ml/kg intraperitoneal injection (i.p.) two times a week for 12 weeks and then saline 1.0 ml/kg per orally on alternate days for two weeks during the 13th -14th week. One week after ascites formation without CCl4, lipid nanocarrier formulation (without VEGF-C) was administered via oral route on alternate days for 2 weeks during the 13th -14th week (vehicle). The E-VEGF-C group, along with CCl4, received E-VEGF-C through the oral route at a dose of 600 μg/kg of the body weight on alternate days for 2 weeks during the 13th -14th week. Ascites was graded as mild, moderate, or severe based on fluid volume. Less than 10 ml was mild, 10-30 ml was moderate, and >30 ml was severe. These rats were sacrificed 48 hrs. after the last dose of saline, vehicle, or E-VEGF-C, after performing the hemodynamic studies.

The two groups were prepared for the PPVL study. PPVL vehicle (PPVL with nanocarriers alone) and PPVL+E-VEGF-C. Non-cirrhotic animal models of portal hypertension were developed using partial portal vein ligation (PPVL), as previously described [48]. Briefly, under isoflurane anesthesia, using a single ligature of 3-0 silk tied around the portal vein, a calibrated constriction was performed with a 19-gauge blunt-tipped needle. The needle was then removed, leaving a calibrated constriction of the portal vein. For the PPVL animals, the two groups were randomized. In the PPVL+vehicle group, the lipid nanocarrier formulation was administered orally on alternate days for 2 week after the PPVL surgery. In the PPVL+E-VEGF-C group, E-VEGF-C was orally administered at a dose of 600 μg/kg of the body weight of the animal on alternate days for 2 weeks one day after the PPVL surgery week. In a few rats, the plasma volume was measured using Evans Blue dye.

***In vivo* biodistribution and half-life studies**

E-VEGF-C (single dose: 300μg/kg) tagged with coumarin-6 dye was administered on day 0 in healthy animals and CCL4 rats after 12 weeks. Rats were euthanized 2 hrs. after a single oral administration of E-VEGF-C for the collection of liver, intestine, mesentery, spleen, lung, and kidney tissues. The tissues were weighed and homogenized with physiological saline, and fluorescence intensity was detected at 520 nm using a spectrofluorometer. Some parts of the tissues were also observed under a fluorescence microscope for visual detection of labeled nanoparticles. The fluorescence intensity values of coumarin were normalized to those of the untreated control rats. Levels of VEGF-C were determined per mg protein of the tissues using the human VEGF-C ELISA kit (Elabsciences, Houston, USA) according to the manufacturer’s protocol.

For plasma half-life studies, after a single oral injection of E-VEGF-C, serial blood samples (300 μl) were collected from the rats in EDTA vials at 10 min, 20 min, 30 min, 1 hr, 5 hr, 10 hr, and 24 hr. After 20 min of incubation at room temperature, blood samples were centrifuged at 1200× *g* for 10 min. The plasma (100-150 μl) was collected, snap frozen, and stored at –80°C. The amount of VEGF-C in each sample was determined using a human VEGF-C ELISA kit, as previously described. Plasma VEGF-C concentration–time data were analyzed at different time points.

Analysis of Plasma Volume

Plasma volume was measured using Evans blue dye as previously described [12]. Briefly, 0.2 ml of Evans Blue (Himedia labs) solution (3 mg) was injected through a jugular vein catheter, followed by saline to clear the dye from the catheter. After five, 1 ml of blood was withdrawn from the femoral artery catheter. The plasma aliquot was diluted ten times in distilled water, and the absorbance was read at 600-nm using a spectrophotometer. Plasma volume (ml) was calculated using the following formula:
Plasma volume (ml) = Absorbance of standard/Absorbance of sample × 10, where the standard was 3 mg of Evans blue dye in 10 ml of plasma diluted by a factor of 10

Analysis of Lymphatic Transport using Tracer dye BODIPY FL-C16

To evaluate lymphatic drainage in the mLVs, a long-chain fluorescent fatty acid (BODIPY, Thermo fisher), known as lymphatic tracer, was administered orally with olive oil in 1:10 ratio with final volume of 200ul. After 2 hr, mesentery tissue was isolated and optically cleared using methyl salicylate. Images of mesenteric lymphatic drainage were obtained using confocal microscopy at 10X (Leica SP8). Six fields from each slide were randomly selected and photographs were taken. Lymphatic drainage was quantified by measuring BODIPY fluorescence intensity inside the LVs using ImageJ. LVs leakage was quantified by measuring BODIPY fluorescence intensity in vicinity to LVsusing ImageJ. Diameter of the mLVs were calculated using ImageJ diameter plugin.

Assessment of Hepatic and Systemic Hemodynamic Parameters

Rats were anesthetized with ketamine hydrochloride (60 mg/kg) and midazolam (3mg/kg) intraperitoneally, fastened to a surgical board, and maintained a constant temperature of 37°C ± 0.5°C. Tracheostomy and endotracheal cannulation (PE-240 catheter; Portex, Minneapolis, MN, USA) were performed to maintain adequate respiration during anesthesia. The femoral artery and ileocolic vein were cannulated with PE-50 catheters to measure mean arterial pressure (mmHg) and portal pressure (PP) (mmHg), respectively. A non-constrictive perivascular ultrasonic transit time flow probe (2PR, 2-mm diameter; Transonic Systems Inc., Ithaca, NY, USA) was placed around the portal vein as close as possible to the liver to measure portal blood flow (PBF) (mL/min). Intrahepatic vascular resistance (IHR) (mmHg $\cdot mL \cdot min^{-1} \cdot g^{-1}$) was calculated as PP/PBF. Blood pressure and flow were registered on a multichannel, computer-based recorder using Chart, version 5.0.1, for Windows software (PowerLab; AD Instruments). Hemodynamic data were collected after a 20-minute stabilization period

Computed tomography analysis

Computed tomography (CT) was performed 48 h after treatment to visualize ascites. The animals were evaluated using Somatom Definition AS plus 128 Acquisition 384 slice reconstruction (Siemens Healthineers, Forchheim, Germany).

In vitro Studies

Isolation of Lymphatic endothelial cells from mesenteric tissue of rat and uptake of E-VEGF-C in vitro

For the isolation of mesenteric LyECs, protocol was adapted from Ribera *et al.*, 2013 with minor moddifaction. Briefly, the rats were anesthetized with ketamine hydrochloride (60 mg/kg) and midazolam (3mg/kg) intraperitoneally. A midline incision was made to perfuse the mesentery with saline by inserting the catheter into the portal vein. Clear mesenteric tissue was extracted and placed in DMEM supplemented with 2% antibiotic and antimycotic solutions. Sterile scissors were used to finely mince the tissue into ~1 mm3 pieces. The minced tissue was centrifuged at 2500 rpm for 10 min at RT and washed

twice with PBS. For in vitro digestion, 0.25% collagenase IV was previously prepared and prewarmed at 37 C, tissue was resuspended in enzyme solution supplemented with 3mM CaCl2 at constant shaking for proper digestion. Following digestion for 30 min at 37 C, the tube was transferred to a biosafety cabinet, passed the digested tissue suspension through a 70 μm strainer placed into a sterile 50 ml tube. Equal amounts of sterile DMEM were passed through a strainer to inactivate the enzyme. The cell suspension was then centrifuged at 1200 rpm for 5 min at 4 °C and washed twice with PBS.
For sorting of LyECs, LyEC-specific primary antibody podoplanin (pdpn, 1:200) and CD31 (1:100) was added in the cell suspension with CD45 and 7AAD, and cells were incubated on ice for 30 mins. After washing, secondary antibody conjugated with fluorochrome was added at a 1:500 dilution and incubated on ice for 30 min. Thereafter, sorting was performed under sterile conditions using a BD FACS Aria, and the cells were collected in EGM-2 media. Collected cells were washed with PBS, resuspended in EGM-2 medium, and seeded on pre-coated fibronectin plates.
The cultured cells were incubated with nanoengineered VEGF-C particles for 30 min at 37 C in 5% CO2. After incubation, the cells were rinsed with PBS to remove the remaining nanoparticles. Cells were then fixed for 7 min at room temperature in the dark using a permeabilization and fixing kit (BD Cytofix/Cytoperm) and washed once with BD perm/wash buffer[29]. Staining was performed with DAPI (4,6-diamidino-2-phenylindole) at a 1:2000 dilution. Fluorescence of coumarin-6 labeled VEGF-C particle and DAPI-stained cells were imaged using an inverted fluorescence microscope (Evos microscope) in the green and blue channels, respectively. Fluorescence was quantified using the ImageJ software.

Assessment of blood and lymphatic vessels by immunohistochemistry and immunofluorescence

Tissues samples were fixed in 10% buffered formalin and processed. Sections of 7-μm-thick paraffin-embedded tissues were heat fixed and deparaffinized at 45 C and rehydrated in a descending ethanol series. Following antigen retrieval by heating for 8 minutes in a microwave with citrate buffer, sections were incubated for 20 minutes with peroxidase 1 solution to quench endogenous peroxidase. Protein blocking was done 3% BSA. Tissue slides were then incubated overnight at 4C in a humid chamber with anti-podoplanin mAb, and staining was completed using the HRP-conjugated mouse/rar/human detection kit and DAB chromogen as a substrate, according to the manufacturer's instructions. Last, sections were counterstained with Hematoxylin and eosin for 1 minutes. The slides were mounted with a coverslip using Mounting Media. In immunofluorescence, after primary antibody incubation, secondary antibody attached to fluorochrome is added for 1 hr at RT and slides were mounted with Vectashield mounting media with DAPI. Six fields from each slide were randomly selected, and photographs were taken using an inverted fluorescent microscope (Nikon Instruments, Inc.) and quantified using ImageJ software. Details of the antibodies used are provided in S Table 4.

Assessment of Bacterial Translocation

GFP labelled salmonella typhimurium were cultured in Luria Broth with ampicillin and 10^9 cells were orally gavaged in rats for 48 hrs. All experiments were performed under sterile conditions. Rats were Anesthetized with ketamine hydrochloride (60 mg/kg) and midazolam (3mg/kg) intraperitoneally, shaved, and the skin was disinfected with alcohol. Subsequently, after midline laparotomy, MLNs were dissected, removed, and weighed in sterile condition. Tissue samples of liver, spleen, and lung were also removed and weighed. All specimens were diluted in phosphate-buffered saline (100uL per 100mg) and homogenized, and suspension was cultured on Luria broth agar with ampicillin and observed after 24 hrs. Presence of GFP positive bacteria using UV transilluminator was considered evidence of BT to different organs. To test the translocation of bacteria in blood, 5 ml of blood was also collected in sterile condition and added to blood culture bottle and incubated at 37 C. After 1 hr. of incubation, 100 ul of blood were collected from culture bottle and spread on LB agar plate and incubated at 37 C.

Immune cell quantification using Flow Cytometry

Cells were isolated from Mesenteric lymph node using enzymatic digestion by collagenase type IV at 37 C for 10 mins and single cell suspension was prepared using 40-micron sterile filter. Rest of the tissue was was passed through the filter using 5 ml syringe plunger. Single cell suspension was washed with PBS and counted. Cells from blood was isolated using RBC lysis buffer. 9 ml of RBC lysis buffer 1X was added to 1 ml of blood and centrifuged at 1500 rpm, 25 C for 5 min. cells were washed with PBS and counted. Half million cells were incubated with antibodies specific for T cell subsets and dendritic cells and incubated for 30 min to 1 hr in dark at 4C. 1 lakh events were acquired for each experiment.

Detection of TNF-α and endotoxins in the Ascitic fluid and Systemic Circulation

TNF-α levels were assessed using a TNF-α ELISA kit (Thermo Fisher Scientific, Massachusetts, USA) as recommended by the manufacturer's protocol. Endotoxin levels in the serum were assessed using a chromogenic kinetic limulus ameobocyte lysate assay kit, following the manufacturer's instructions **(**Thermo Fisher Scientific, Massachusetts, USA).

RNA extraction and RT-PCR

RNA extraction and RT-PCR were performed on excised mesenteric tissues stored in an RNA buffer. Total RNA was isolated using a Nucleopore kit, according to the manufacturer's instructions. RNA was quantified at 260/280 nm using a Nanodrop 2000 spectrophotometer (Thermo Scientific). First-strand cDNA was synthesized from 1µg of total RNA using reverse transcriptase (Thermo Fisher Scientific Verso cDNA synthesis kit) according to the manufacturer's instructions. Quantitative real-time PCR was performed using SYBR green PCR master mix (Fermentas Life Sciences) on a ViiA7 instrument PCR system (Applied Biosystems, USA). The following cycling parameters were used: start at 95 °C for 5 min, denaturation at 95 °C for 30 s, annealing at 60 °C for 30 s, elongation at 72 °C for 30 s, and a final 5 min extra extension at the end of the reaction to ensure that all amplicons were completely extended and repeated for 40 amplification cycles. Relative quantification of the expression of relevant genes was performed using the ΔΔCt method after normalization to the expression of the housekeeping gene GAPDH. Primer sequences used are listed in S Table S5.

Western Blotting

Mesenteric tissues were crushed in liquid nitrogen, and 100 mg of tissue powder was added to 200 µL of RIPA lysis buffer (Merck, sigma 20-188). Homogenization was performed on ice until a clear solution was obtained. After centrifugation at 12,000 rpm for 20 min, the supernatant was collected in fresh microcentrifuge tubes and incubated on ice for 30 min. The protein content of the tissue lysate was measured using a BCA kit (Thermo Fisher Scientific, Waltham, MA, USA). Protein samples were denatured at 95°C for 5' in Laemmli buffer. 60 µg of protein was loaded into each well and separated by 10% SDS-PAGE. The gel was run at 80 V for approximately 2 hr. Proteins were electroblotted onto activated PVDF membrane at 60 V for 2 hr. at 4°C, and the membrane was blocked in 5% BSA in Tris-buffered saline containing 0.05% Tween for 2 hr. Membranes were blotted with various primary antibodies i.e., VEGF-C and GAPDH overnight at 4°C, followed by the appropriate HRP-conjugated anti-rabbit and anti-mouse secondary antibodies for 2 hr. The membrane was then treated with the chemiluminescence ECL, and visualized on gel doc (Invitrogen, iBrightCL1500). Densitometry was performed using NIH software (ImageJ). Details of the antibodies used are provided in S Table 4.

Statistical Analysis

Continuous variables are expressed as either mean ± standard deviation for continuous distribution or as median values for skewed distribution. Continuous variables were compared between the two groups using an unpaired two-tailed Student's t-test or Mann-Whitney U test. Variables greater than 2 were compared using one-way ANOVA followed by a post hoc Tukey test. Bar diagrams with various data points, dot plots, and box whisker plots were plotted using GraphPad Prism (version 8.0.1.; GraphPad Software, San Diego, CA, USA), and statistical analysis was performed using GraphPad Prism. Statistical significance was set at $p < 0.05$.

Data Availability

All the data supporting the findings of this study are available within the article and its supplementary information files and from the corresponding authors upon reasonable request.

Acknowledgements

The authors would like to thank Department of Science and Technology (DST), Ministry of Science & Technology, Government of India (DST/NM/NT/2019/191) for the financial support and Center for Nanotechnology (CNT) and the North East Centre for Biological Sciences and Healthcare Engineering (NECBH) of IIT-Guwahati, Assam, India, for providing the facility for AFM and FE-SEM analysis.

References:

1. Sepanlou, S. G. *et al.* The global, regional, and national burden of cirrhosis by cause in 195 countries and territories, 1990–2017: a systematic analysis for the Global Burden of Disease Study 2017. *Lancet Gastroenterol. Hepatol.* **5**, 245–266 (2020).
2. Asrani, S. K., Devarbhavi, H., Eaton, J. & Kamath, P. S. Burden of liver diseases in the world. *J. Hepatol.* **70**, 151–171 (2019).
3. D'Amico, G., Bernardi, M. & Angeli, P. Corrigendum to 'Towards a new definition of decompensated cirrhosis' [J Hepatol 76 (2022) 202-207]. *J. Hepatol.* **76**, 757 (2022).
4. Albillos, A., de Gottardi, A. & Rescigno, M. The gut-liver axis in liver disease: Pathophysiological basis for therapy. *Journal of Hepatology* vol. 72 558–577 (2020).
5. Fukui, H. Leaky Gut and Gut-Liver Axis in Liver Cirrhosis: Clinical Studies Update. *Gut Liver* **15**, 666–676 (2021).
6. Cifarelli, V. & Eichmann, A. The Intestinal Lymphatic System: Functions and Metabolic Implications. *Cell. Mol. Gastroenterol. Hepatol.* **7**, 503–513 (2019).
7. Bernier-Latmani, J. & Petrova, T. V. Intestinal lymphatic vasculature: Structure, mechanisms and functions. *Nature Reviews Gastroenterology and Hepatology* vol. 14 510–526 (2017).
8. Hong, J. W., Park, H. E., Shin, M. J., Shin, Y. B. & Yoon, J. A. Secondary lymphedema after intestinal tuberculosis: A case report. *Ann. Rehabil. Med.* **43**, 725–729 (2019).
9. Danese, S. Role of the vascular and lymphatic endothelium in the pathogenesis of inflammatory bowel disease: 'Brothers in arms'. *Gut* vol. 60 998–1008 (2011).
10. Dunbar, B. S., Elk, J. R., Drake, R. E. & Laine, G. A. Intestinal lymphatic flow during portal venous hypertension. *Am. J. Physiol. - Gastrointest. Liver Physiol.* **257**, (1989).
11. Chung, C. & Iwakiri, Y. The lymphatic vascular system in liver diseases: its role in ascites formation. *Clinical and molecular hepatology* vol. 19 99–104 (2013).

12. Ribera, J. *et al.* Increased nitric oxide production in lymphatic endothelial cells causes impairment of lymphatic drainage in cirrhotic rats. *Gut* **62**, 138–145 (2013).
13. Nurmi, H. *et al.* VEGF C is required for intestinal lymphatic vessel maintenance and lipid absorption . *EMBO Mol. Med.* **7**, 1418–1425 (2015).
14. Güç, E. *et al.* Local induction of lymphangiogenesis with engineered fibrin-binding VEGF-C promotes wound healing by increasing immune cell trafficking and matrix remodeling. *Biomaterials* **131**, 160–175 (2017).
15. Bouta, E. M. *et al.* Targeting lymphatic function as a novel therapeutic intervention for rheumatoid arthritis. *Nature Reviews Rheumatology* vol. 14 94–106 (2018).
16. Hagura, A. *et al.* The VEGF-C/VEGFR3 signaling pathway contributes to resolving chronic skin inflammation by activating lymphatic vessel function. *J. Dermatol. Sci.* **73**, 135–141 (2014).
17. Hsu, S. J. *et al.* Enhanced Meningeal Lymphatic Drainage Ameliorates Neuroinflammation and Hepatic Encephalopathy in Cirrhotic Rats. *Gastroenterology* **160**, 1315-1329.e13 (2021).
18. Lohela, M., Saaristo, A., Veikkola, T. & Alitalo, K. Lymphangiogenic growth factors, receptors and therapies. *Thrombosis and Haemostasis* vol. 90 167–184 (2003).
19. Claaßen, C., Sewald, L., Tovar, G. E. M. & Borchers, K. Controlled Release of Vascular Endothelial Growth Factor from Heparin-Functionalized Gelatin Type A and Albumin Hydrogels. *Gels* **3**, (2017).
20. Geng, H., Song, H., Qi, J. & Cui, D. Sustained release of VEGF from PLGA nanoparticles embedded thermo-sensitive hydrogel in full-thickness porcine bladder acellular matrix. *Nanoscale Res. Lett.* **6**, (2011).
21. JM, V. *et al.* The cardiac lymphatic system stimulates resolution of inflammation following myocardial infarction. *J. Clin. Invest.* **128**, 3402–3412 (2018).
22. Úbeda, M. *et al.* Critical role of the liver in the induction of systemic inflammation in rats with preascitic cirrhosis. *Hepatology* **52**, 2086–2095 (2010).
23. Wiest, R., Lawson, M. & Geuking, M. Pathological bacterial translocation in liver cirrhosis. *J. Hepatol.* **60**, 197–209 (2014).
24. Zhang, L. *et al.* Implications of lymphatic alterations in the pathogenesis and treatment of inflammatory bowel disease. *Biomed. Pharmacother.* **140**, 111752 (2021).
25. Rossi, P. *et al.* Intestinal lymphangiectasia in adults. *World J. Gastrointest. Oncol.* **3**, 19 (2011).
26. Zhang, L. *et al.* Implications of lymphatic alterations in the pathogenesis and treatment of inflammatory bowel disease. *Biomed. Pharmacother.* **140**, 111752 (2021).
27. Schwager, S. *et al.* Antibody-mediated delivery of VEGF-C potently reduces chronic skin inflammation. *JCI insight* **3**, (2018).
28. Szőke, D. *et al.* Nucleoside-modified VEGFC mRNA induces organ-specific lymphatic growth and reverses experimental lymphedema. *Nat. Commun. 2021 121* **12**, 1–18 (2021).
29. Banerjee, S. & Pillai, J. Solid lipid matrix mediated nanoarchitectonics for improved oral bioavailability of drugs. *Expert Opin. Drug Metab. Toxicol.* **15**, 499–515 (2019).
30. BIPHASIC DRUG DELIVERY IN CONTROLLED RELEASE FORMULATIONS – A REVIEW | Srinivasa Rao Avanapu - Academia.edu. https://www.academia.edu/17705231/BIPHASIC_DRUG_DELIVERY_IN_CONTROLLED_RELEASE_FORMULATIONS_A_REVIEW.
31. Banerjee, S., Roy, S., Bhaumik, K. N. & Pillai, J. Mechanisms of the effectiveness of lipid nanoparticle formulations loaded with anti-tubercular drugs combinations toward overcoming drug bioavailability in tuberculosis. *J. Drug Target.* **28**, 55–69 (2020).
32. Deng, Y., Zhang, X. & Simons, M. Molecular controls of lymphatic VEGFR3 signaling. *Arterioscler. Thromb. Vasc. Biol.* **35**, 421–429 (2015).
33. Breslin, J. W. *et al.* Vascular endothelial growth factor-C stimulates the lymphatic pump by a VEGF receptor-3-dependent mechanism. *Am. J. Physiol. Heart Circ. Physiol.* **293**, (2007).
34. D'Alessio, S. *et al.* VEGF-C-dependent stimulation of lymphatic function ameliorates experimental inflammatory bowel disease. *J. Clin. Invest.* **124**, 3863–3878 (2014).

35. Visuri, M. T. *et al.* VEGF-C and VEGF-C156S in the pro-lymphangiogenic growth factor therapy of lymphedema: a large animal study. *Angiogenesis* **18**, 313–326 (2015).
36. Cabrera, J. *et al.* Abdominal decompression plays a major role in early postparacentesis haemodynamic changes in cirrhotic patients with tense ascites. *Gut* **48**, 384–389 (2001).
37. Geerts, A. M. *et al.* Increased angiogenesis and permeability in the mesenteric microvasculature of rats with cirrhosis and portal hypertension: An in vivo study. *Liver Int.* **26**, 889–898 (2006).
38. Santambrogio, L., Berendam, S. J. & Engelhard, V. H. The antigen processing and presentation machinery in lymphatic endothelial cells. *Front. Immunol.* **10**, 1033 (2019).
39. Macpherson, A. J. & Smith, K. Mesenteric lymph nodes at the center of immune anatomy. *J. Exp. Med.* **203**, 497–500 (2006).
40. Wiest, R., Lawson, M. & Geuking, M. Pathological bacterial translocation in liver cirrhosis. *J. Hepatol.* **60**, 197–209 (2014).
41. G, G.-T., FY, L., GE, B., R, C. & AB, W. Bacterial translocation to mesenteric lymph nodes is increased in cirrhotic rats with ascites. *Gastroenterology* **108**, 1835–1841 (1995).
42. Vieira, J. M. *et al.* The cardiac lymphatic system stimulates resolution of inflammation following myocardial infarction. *J. Clin. Invest.* **128**, 3402–3412 (2018).
43. Dieterich, L. C., Seidel, C. D. & Detmar, M. Lymphatic vessels: new targets for the treatment of inflammatory diseases. *Angiogenesis* **17**, 359–371 (2014).
44. Bairagi, U., Mittal, P., Singh, J. & Mishra, B. Preparation, characterization, and in vivo evaluation of nano formulations of ferulic acid in diabetic wound healing. *Drug Dev. Ind. Pharm.* **44**, 1783–1796 (2018).
45. Nguyen, T. B. T., Li, S. & Deratani, A. Reverse micelles prepared from amphiphilic polylactide-b-poly(ethylene glycol) block copolymers for controlled release of hydrophilic drugs. *Int. J. Pharm.* **495**, 154–161 (2015).
46. O'Dwyer, J. *et al.* Development of a nanomedicine-loaded hydrogel for sustained delivery of an angiogenic growth factor to the ischaemic myocardium. *Drug Deliv. Transl. Res.* **10**, 440–454 (2020).
47. Kordbacheh, E., Nazarian, S., Hajizade, A. & Farhang, A. Entrapment of HETS recombinant protein onto PLGA and alginate NPs improves the immunogenicity of the protein against E. coli O157:H7. *Mol. Immunol.* **114**, 612–619 (2019).
48. Tripathi, D. M. *et al.* Simvastatin Prevents Progression of Acute on Chronic Liver Failure in Rats With Cirrhosis and Portal Hypertension. *Gastroenterology* **155**, 1564–1577 (2018).

Figure legends:

Figure 1: Mesenteric Lymphatic vessels (mLVs) density increased in liver cirrhosis. (A) Immunohistochemical staining with an antibody recognizing podoplanin was performed in mesentery tissue of control and CCl4 animal model of liver cirrhosis. Scale bar: 500µm. **(B)** The number of the podoplanin positive mLVs was quantified using ImageJ. *P*=0.0240. **(C)** The diameter of the mLVs in control and CCl4 rats was measured using ImageJ's diameter plugin. n=5 each. Data is expressed as mean ± SD. *P*=0.0119 (**D)** mRNA level for Prox1, LyVE1, VEGF-C, CCL21, eNOS, and COX2 were quantified in mesentery tissue using qRT-PCR. n=5 each. Data is expressed as mean ± SD. Two-tailed unpaired T-test. *P*=0.05-0.01 compared to control, where the dotted line represents control. **(E)** Immunofluorescence staining for antibody recognizing VEGFR3 and DAPI for nuclear staining was performed in mesentery tissue of control and CCl4 rats. Scale bar: 186.2µm**. (F)** VEGFR3 expression was quantified from the same sections using ImageJ. Data is expressed as mean ± SD. n=5 each. Two-tailed, unpaired T-test, *P*=0.0147. '*' represents p< 0.05.

Figure 2: Formation and characterization of nanoengineered E-VEGF-C. (A) Schematic representation of VEGF-C-engineered stealth nano-lipocarriers (E-VEGF-C). Histograms showing **(B)** Mean Particle Size (MPS), Polydispersity Index (PDI), and **(C)** zeta potential of E-VEGF-C. **(D)** Field emission-scanning electron microscope (FE-SEM) and of E-VEGF-C. Surface morphology and size of E-VEGF-C were visualized using FE-SEM at 4.70 K X and 50.67 KX magnification. **(E)** Field emission-transmission electron microscopy (FE-TEM) analysis of E-VEGF-C The morphology and size of E-VEGF-C were examined using FE-TEM, indicating a spherical shape. **(F)** Atomic force microscopy (AFM) micrographs provide two-dimensional (2D) and three-dimensional (3D) images of E-EVGF-C surface morphology as compact, smooth, and spherical in shape. The average diameter of an individual particle of the prepared E-VEGF-C was 16 nm. (**G)** *In vitro* release profile of E-VEGF-C in PBS at pH 7.4. An initial burst release of 31.95 ± 1.52 % VEGF-C was observed at 2 hr post mixing, followed by an increase in VEGF-C release of 84.66 ± 1.82 % at 4 hr, which gradually decreased at post-mixing time points.

Figure 3: *In vitro* and *in vivo* uptake and biodistribution of E-VEGF-C. (A) Primary lymphatic endothelial cells (LyECs) were cultured and incubated with coumarin-6 labelled E-VEGF-C and observed at different time points. Scale bars: 100µm. **(B)** Line graph of the coumarin positive LyECs depicting the percentage of E-VEGF-C uptake at different time points. **(C)** Schema of *in vivo* biodistribution studies. 300ug/kg of coumarin labelled E-VEGF-C was given orally in control and CCl4 rats. n=6 each. All tissues were collected 2 hrs. after gavage and measured for fluorescence in fluorimeter. **(D)** Representative fluorescence images of mesentery tissue section of control and CCl4-V rats showing localization of coumarin tagged E-VEGF-C in gut. Scale bars: 200µm. **(E)** Quantitative fluorescence analysis in different tissue of control and CCl4 rats using fluorimeter. Data is expressed as mean ± SD.

n=6 each group. **(F)** ELISA of human VEGF-C (pg/mg of total protein) in different tissue of control and CCl4 rats. n=3 each. *P*=0.01-0.001 **(G)** Levels of human VEGF-C (pg/ml) in control and CCl4-V rat plasma samples at indicated time points were measured using ELISA. n=3 each. Data is expressed as mean ± SD. '*' represents p< 0.05 and '**' represents p< 0.01

Figure 4: Effect of E-VEGF-C treatment on mesenteric lymphatic vessels (mLVs) in cirrhotic rat model of portal hypertension (PHT). (**A)** Schema of the *in vivo* studies. CCl4 rats were treated with E-VEGF-C 600ug/kg on alternate days for 2 weeks after ascites formation. n=8 each group. **(B)** Immunohistochemistry staining for antibody recognizing podoplanin (pdpn) in the mesenteric tissue sections of CCl4-V and E-VEGF-C treated rat. Scale bars: 500µm. Arrow indicated at pdpn+ LVs. (**C)** The number of pdpn+ mLVs were quantified using ImageJ**.** n=5 or 6 rats per group. Data is expressed as mean ± SD. Unpaired two-tailed T-test were performed. *P* > 0.05. (**D)** The diameter of pdpn+ mLVs from the same sections was measured using ImageJ diameter plugin. n=5 or 6 rats in each group. Data is expressed as mean ± SD. Unpaired two-tailed T-test were performed. *P*=0.0073. **(E)** Immunohistochemical staining for antibody recognizing pdpn was performed on mesenteric lymph node (MLN) section of control, CCl4, and E-VEGF-C treated rats. **(F)** Brown areas were quantified as IHC scores using ImageJ**.** n=5 each. Data is expressed as mean ± SD. One-way ANOVA with Tukey's post-hoc test was performed. *P*=0.0197 for Control vs CCl4-V and *P*=0.0346 for CCl4-V vs E-VEGFC. (**G)** The expression of human VEGF-C protein was measured using western blotting in control, CCl4, and E-VEGF-C. (**H)** Quantitative analysis of the western blot is represented in the bar graph. The dotted line represents control. n=4 each. Data is expressed as mean ± SD. '*' represents p< 0.05, '**' represents p< 0.01, and '***' represents p< 0.001.* represent comparison with control.

Figure 5: Effect of E-VEGF-C on proliferation and drainage of mLVs. (**A)** Whole-mount immunostaining of mLVs of control, CCl4, and E-EVGF-C rats was performed with an antibody recognizing podoplanin. The upper 2 panels represent mesenteric collecting LVs, and the lower 2 panels represent lymphatic capillaries entering the intestine. Scale bar:309.4µm. (**B)** The diameter of the collecting mLVs were measured from the same section using ImageJ diameter plugin. n=3 or 4 rats in each group. Data is expressed as mean ± SD One Way ANOVA with post hoc Tukey's test was performed. *P*<0.0001 for control vs. CCl4-V and *P*=0.0183 for CCl4-V vs. E-VEGF-C (**C)** Mesentery tissue of CCl4-V and E-VEGF-C rats. Arrowheads indicated the proliferation and branching of mLVs in mesentery of E-EVGF-C treated rat. (**D)** Quantitative analysis of branching points in the mesentery of control, CCl4, and E-VEGF-C rats. n=3-4 rats in each group. Data is expressed as mean ± SD. One Way ANOVA with post hoc Tukey's test was performed. *P*>0.05 for each comparison. **(E)** Workflow for visualization of mLVs by oral gavaging of BODIPY FL-C16. (**F)** Corresponding images of mLVs after BODIPY FL-C16 administration in control, CCl4-V, and E-VEGF-C treated rats. Scale bar:309.1µm Representative graphs for characterization of LVs. The mean of three points from each field was taken. **(G)** Diameter of LVs was measured in µm using ImageJ diameter plugins. (**H)** Drainage of LVs was measured by fluorescence inside the vessels using ImageJ by quantifying the mean intensity of BODIPY. 100 –mean intensity percentage was plotted in the graph. (**I)** Quantification of lymph leakage from vessels by measuring the mean fluorescence intensity of BODIPY in extraluminal space**.** n=4 or 5 rats in each group. Data is expressed as mean ± SD. '***' represents p<0.001, and '*' represents p<0.05.

Figure 6: Effect of E-VEGF-C treatment on ascitic fluid volume and hemodynamic parameters in CCl4 and Partial Portal Vein Ligation (PPVL) rat model. (A) Representative CT scan slices of all study groups showing the abdominal cavity. The regions of interest are marked with a red dotted outline and correspond to the zones with the accumulation of fluid. **(B)** Dot plots showing ascitic fluid volume (ml) in the CCl4-V and E-EVGF-C treated rats. n=6 each group. Data is expressed as mean ± SD. Unpaired two-tailed t-test were performed, *P*=0.0168. (**C)** Histograms showing plasma volumes (ml) in all study groups measured using the Evans Blue dye dilution technique. n=4 each. (**D)** Bar Diagrams

showing hepatic hemodynamic parameters, Portal pressure (PP), Portal Blood Flow (PBF), and Intrahepatic resistance (IHR) in the study groups n=6 each. Data is expressed as mean ± SD. One Way ANOVA with post hoc Tukey's test was performed. $P<0.05$ **(E)** Masson Trichrome (MT) stained images (10x) of liver tissues in different animal groups. Liver fibrosis was assessed using the Laennec fibrosis scoring system. (**F)** Bar Diagrams showing hepatic hemodynamic parameters Portal pressure (PP), Portal Blood Flow (PBF), and Intrahepatic resistance (IHR) in control, PPVL vehicle and PPVL+E-VEGF-C rats. n=5 each Data is expressed as mean ± SD. Unpaired two-tailed t-test were performed. '*' represents p< 0.05 and '**' represents p< 0.01, and '***' represents p< 0.001. *Represent comparison with control.

Figure 7: Effect of E-EVGF-C on gene expression profiling of lymphatic endothelial cells (LyECs). (A) Schema of workflow. LyECs were isolated from mesentery and MLNs of all study groups using FACS. RNA isolation and qRT-PCR analysis were done for different marker genes of LyECs. **(B)** Relative gene expression of LyVE1, Prox1, VCAM1, VE-Cad, MHCII, CD86, CCL21, and COX2 genes in CCl4-V and E-VEGF-C treated rats were plotted. Dotted lines represent Control. n= 3 each. Data is expressed as mean ± SD. One Way ANOVA with post hoc Tukey's test was performed. '**' represents p<0.01, '*' represents p<0.05. *Represent comparison with CCl4-V.

Figure 8: Effect of E-VEGF-C on priming of immune cells and clearance of bacterial load. (A-E) Immune cell quantification using flow cytometry. Cells were isolated from the mesenteric lymph node of control, CCl4 and E-VEGF-C rats and stained with antibodies for T cells subsets and Dendritic cells. Acquisition of 1 lakh events was performed in each experiment. (**A)** Dot Plots of T cells subsets in MLN of control, CCl4-V, and E-VEGF-C. **(B)** Percentage population of CD3 T cells, CD4 helper T cells, CD8 cytotoxic T cells, CD134+ recently activated helper and cytotoxic T cells. **(C)** Dot plots of CD25+ regulatory helper T cells in all study groups. **(D)** Percentage population of T regulatory cells positive for CD3, CD4/CD8, and CD25. (**E)** Percentage population of dendritic cells (DCs) positive for CD11c, CD103, and CD80. n=5 each. Data is expressed as mean ± SD. One Way ANOVA with post hoc Tukey's test was performed. $P<0.05$ **(F)** Schema of workflow where 10^9 GFP+ bacteria were given to rats orally, and tissue were collected in sterile condition after 48hrs of gavage. 100 mg of MLN tissue were homogenized in PBS and spread on LB agar plates for bacterial load quantification. Cells were isolated from MLNs for immune cell quantification using flow cytometry. (**G)** GFP labelled *S. typhimurium* colonies in 100 mg of MLN tissue extract of each group visualized using a UV transilluminator. (**H)** Quantitative analysis of CFU/gm of MLN tissue for GFP labelled *S. typhimurium.* n=3 each. Data is expressed as mean ± SD. One Way ANOVA with post hoc Tukey's test was performed. $P<0.001$. **(I)** Dot Plots of T cells subsets in cells isolated from MLNs of all study groups after bacterial challenge. **(J)** Percentage population of CD4 helper T cells, CD8 cytotoxic T cells, CD134+ recently activated helper, and cytotoxic T cells. **(K)** Dot plots of CD25+ regulatory helper T cells. **(L)** Percentage population of T regulatory cells positive for CD3, CD4/CD8, and CD25. n=4 each. Data is expressed as mean ± SD. One Way ANOVA with post hoc Tukey's test was performed. '#' represents comparison with control. '*' represent a comparison with CCl4-V. '***' represents p<0.001, '**' represents p<0.01, and '*' represents p<0.05. '#' represents p<0.05.

Figure 9: Effect of E-EVGF-C on systemic inflammation. Quantification of endotoxins and TNF-α in serum and ascitic fluid of control, CCl4-V, and E-VEGF-C rats. Dot plots showing levels of Endotoxins (EU/ml) **(A)** in serum and (**B)** ascitic fluid. Dot plots showing levels of TNF-α (pg/ml) **(C)** in serum and **(D)** in ascitic fluid. n=4 each. Data is expressed as mean ± SD. '*' represents p< 0.05, and '**' represents p<0.01.

Supplementary Figure legends:

Supp Figure 1: Schematic diagram for the preparation of reverse micelles: Preparation of nanoengineered Distearoyl-rac-glycerol-PEG2K (DSG-PEG) based reverse micelles loaded with human recombinant VEGF-C (Cys56Ser) using homogenization.

Supp Figure 2: Sorting and culture of mesenteric lymphatic endothelial cells (LyECs). (A) Primary cells were isolated from rat mesentery and labelled with CD31 and Pdpn antibodies for sorting LyEC using FACS. Dot plot graph showing the gating for sorting LyECs positive for CD31 and Pdpn. (**B)** Culture of sorted LyECs on the fibronectin-coated dish. Magnification 20x. (**C)** Ex vivo bio-distribution of coumarin-6 tagged E-VEGF-C in control and CCl4 rats after 2 hours of E-VEGF-C administration via the oral route. Scale bar: 500µm.

Supp Figure 3: (A) Hematoxylin and Eosin staining of control, CCl4-V, and E-VEGF-C mesentery sections. E-VEGF-C treated rats showed less immune cell infiltration and inflammation compared to the CCL4-V rat mesentery section indicated by the arrow. **(B)** Relative gene expression of eNOS, iNOS, bFGF, COX2, and CCL21 in mesentery tissue with mesenteric lymph node extract in all study groups. The dotted line represents control. n=4 each. Data is expressed as mean ± SD. **(C)** Immunofluorescence staining of an antibody recognizing CD31 in mesentery tissue section. DAPI is used for nuclear staining. (**D)** Quantitative analysis of the CD31+ blood vessels in mesentery of CCl4-V and E-VEGF-C treated. n=4 each. Data is expressed as mean ± SD. ns= non-significant, '*' represents $p< 0.05$ and '**' represents $p< 0.01$, and '***' represents $p< 0.001$

Supp Figure 4: Bar Diagrams showing hepatic hemodynamic and physiological parameters such as Mean Arterial Pressure (MAP), Beats/min, Superior Mesenteric Artery Blood Flow (SMABF), Liver weight, and Body weight in all study groups. n=6 each. Data is expressed as mean ± standard deviation. One Way ANOVA with post hoc Tukey's test was performed '*' represents $p< 0.05$ and '**' represents $p< 0.01$, and '***' represents $p< 0.001$

Supp Figure 5: Effect of E-VEGF-C treatment on mesenteric lymphatic vessels in non-cirrhotic rat model of portal hypertension. (**A)** Schema of the *in vivo* studies. Partial Portal Vein Ligation (PPVL) was done in rats to develop portal hypertension without cirrhosis. One week after surgery, rats were treated with E-VEGF-C 600ug/kg on alternate days for 2 weeks. n=6 each group. (**B)** Hematoxylin and Eosin staining of liver and mesentery tissue section of PPVL rats treated with Vehicle or E-EVGFC. Scale bar: 500um. (**C)** Immunohistochemistry staining for antibody recognizing VEGFR3 in the mesenteric tissue sections of PPVL-Veh and PPVL+E-EVGF-C. Scale bars represent 500µm. Arrow indicated at VEGFR3+LVs. (**D)** Quantitative analysis of the same section. VEGFR3+ LVs were counted and plotted. n=5 each. Data is expressed as mean ± SD. Unpaired two-tailed t-test were performed. P=0.0352. (**E)** The expression of human VEGF-C protein was measured using Western Blotting in control, PPVL-Veh, and PPVL+E-VEGF-C treated rats. **(F)** Quantitative analysis of the western blot is represented in bar graph. Dotted lines represent control. n=4 each. Data is expressed as mean ± SD. (**G)** Relative gene expression of bFGF, CCL21, iNOS, and eNOS and in mesentery tissue with mesenteric lymph node extract of PPVL-Vehicle and PPVL-E-EVGF-C rats. Dotted lines represent control. n=4 each. Data is expressed as mean ± SD. One Way ANOVA with post hoc Tukey's test was performed. '*' represents $p< 0.05$, '**' represent $p<0.01$ and '***' represents $p< 0.001$.

Supp Figure 6: (A) Schema representation of the workflow. Cells were isolated from the mesenteric lymph node of control, CCl4-V, and E-VEGF-C treated rats and labelled with antibodies for T cell subsets and Dendritic cells. **(B)** Gating strategy for the flow cytometry quantification of T cell subsets and Dendritic cells. 1 lakh events were acquired for each experiment. **(C)** GFP labelled Salmonella typhimurium 10^9 bacteria were orally given in control, CCl4 and E-VEGF-C treated rats and tissue were collected after 48 hrs. 100 mg of Liver, Spleen, and Lung were homogenized and plated on LB agar plate. Blood was collected and transferred to a blood culture bottle and incubated for 1 hr. in 37 C. 100 ul of

blood was collected from the blood culture bottle using a sterile syringe and plated on LB agar plate. Plates were observed in UV transilluminator after 24 hrs. of incubation at 37 C.

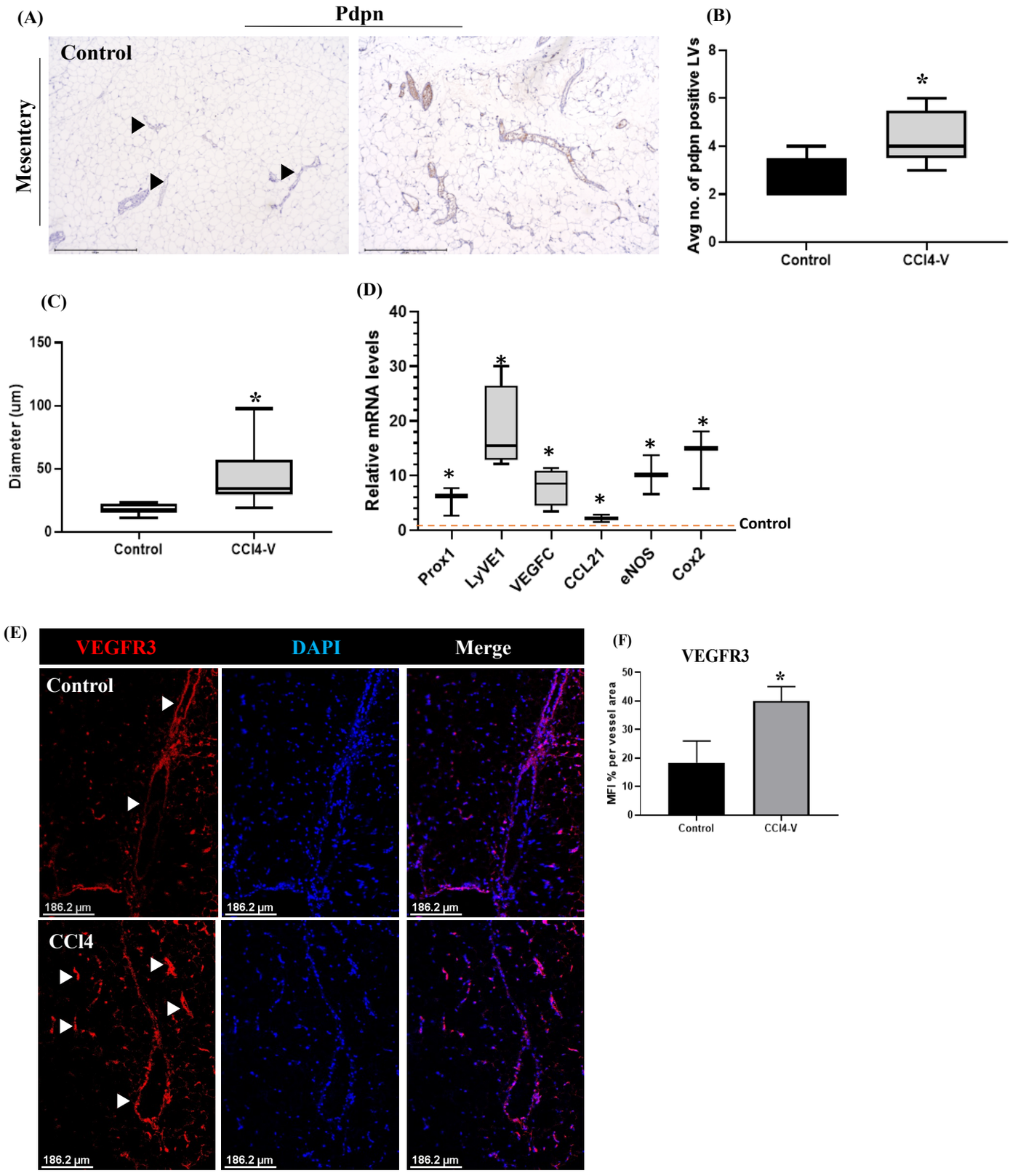
(A)
Pdpn
Control
Mesentery
(B)
Avg no. of pdpn positive LVs
Control
CCl4-V
(C)
Diameter (um)
Control
CCl4-V
(D)
Relative mRNA levels
Control
Prox1
LyVE1
VEGFC
CCL21
eNOS
Cox2
(E)
VEGFR3
DAPI
Merge
Control
CCl4
186.2 µm
(F)
VEGFR3
MFI % per vessel area
Control
CCl4-V

(A)

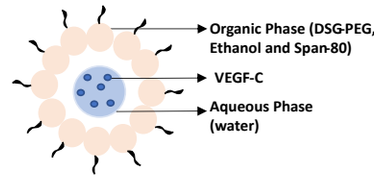

E-VEGF-C

(B) **MPS: 134.8 ± 0.47 nm**
PDI: 0.126 ± 0.01

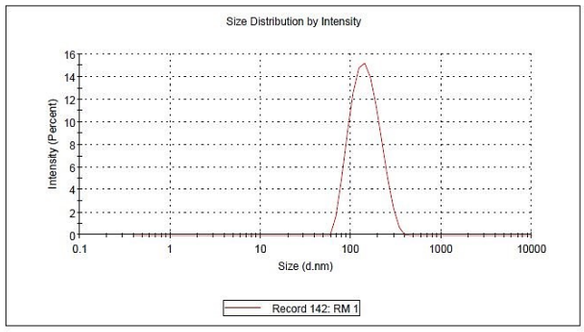

(C) **Zeta potential: -21.9 ± 1.24 mV**

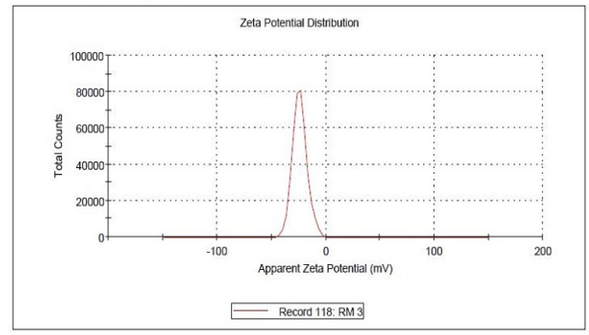

(D) **FE-SEM**

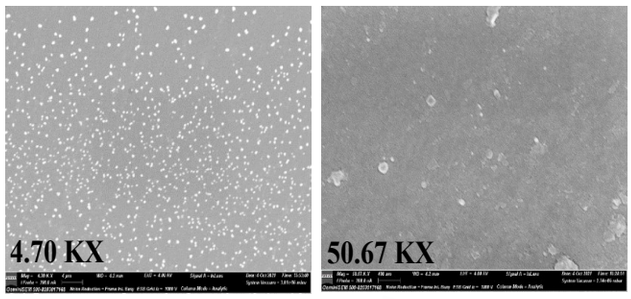

(E) **FE-TEM**

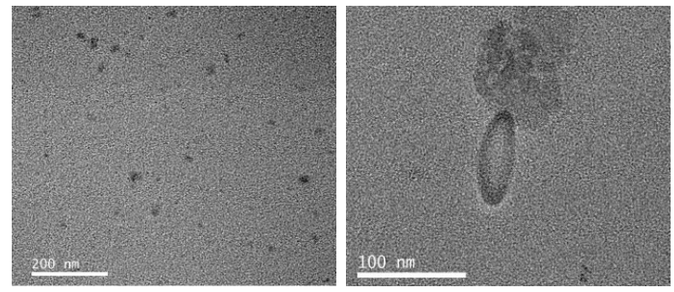

(F) **2D and 3D AFM**

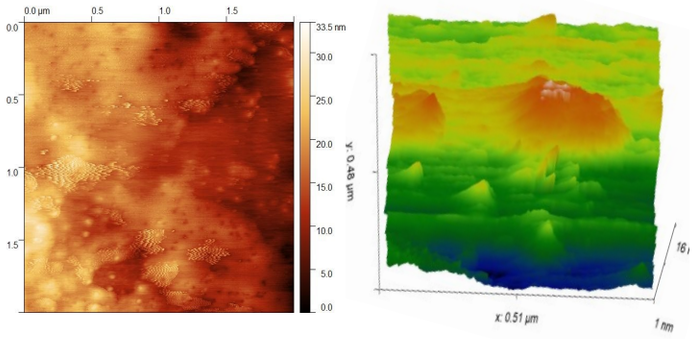

(G)

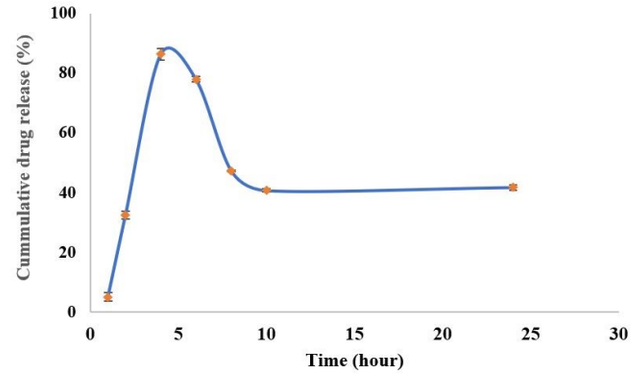

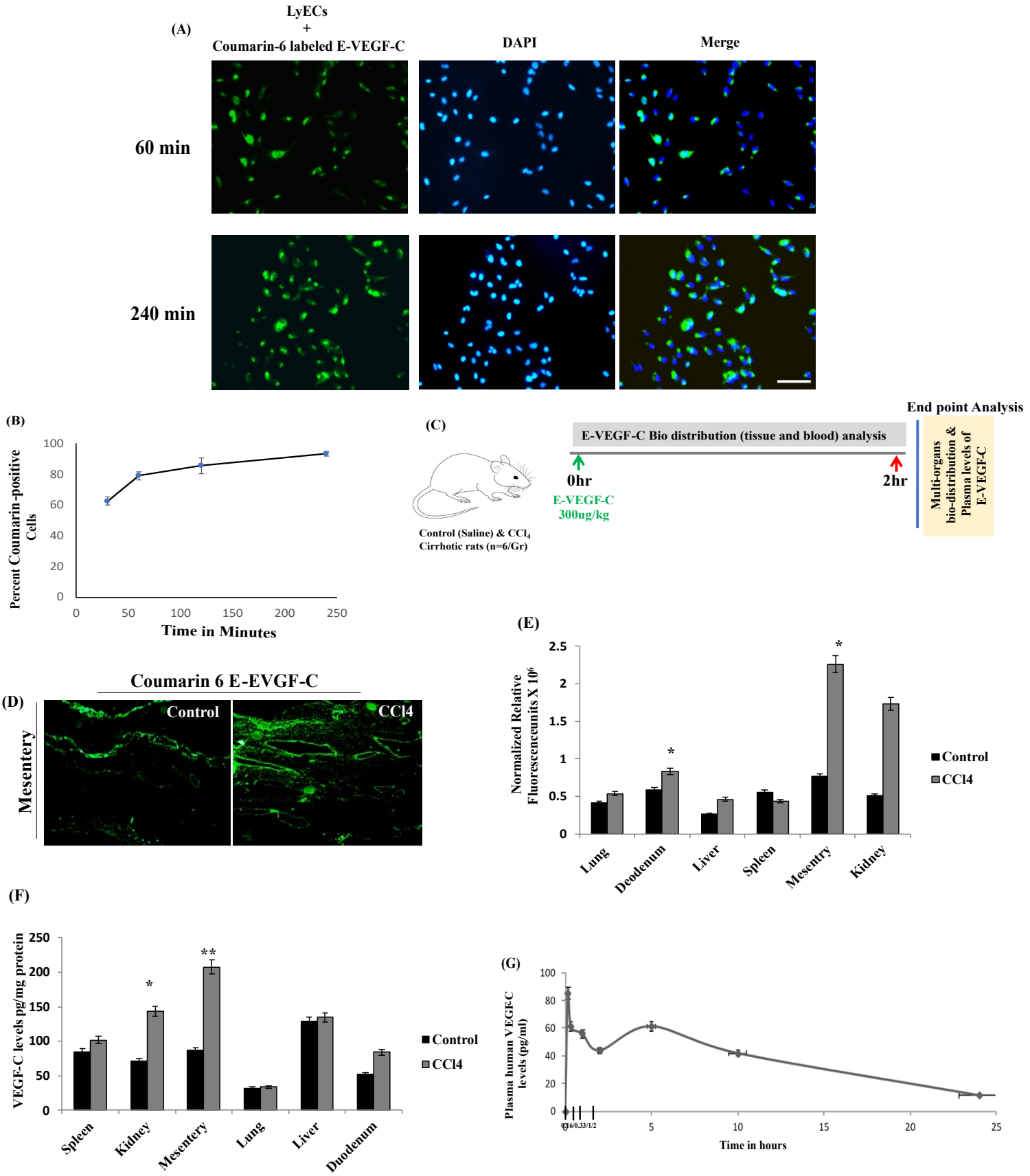
(A)
LyECs
+
Coumarin-6 labeled E-VEGF-C
DAPI
Merge
60 min
240 min
(B)
Percent Coumarin-positive Cells
Time in Minutes
(C)
Control (Saline) & CCl4
Cirrhotic rats (n=6/Gr)
E-VEGF-C Bio distribution (tissue and blood) analysis
0hr
E-VEGF-C
300ug/kg
2hr
End point Analysis
Multi-organs bio-distribution & Plasma levels of E-VEGF-C
(D)
Coumarin 6 E-EVGF-C
Mesentery
Control
CCl4
(E)
Normalized Relative Fluorescenceunits X 10^6
Control
CCl4
Lung
Deodenum
Liver
Spleen
Mesentry
Kidney
(F)
VEGF-C levels pg/mg protein
Control
CCl4
Spleen
Kidney
Mesentery
Lung
Liver
Duodenum
(G)
Plasma human VEGF-C levels (pg/ml)
Time in hours

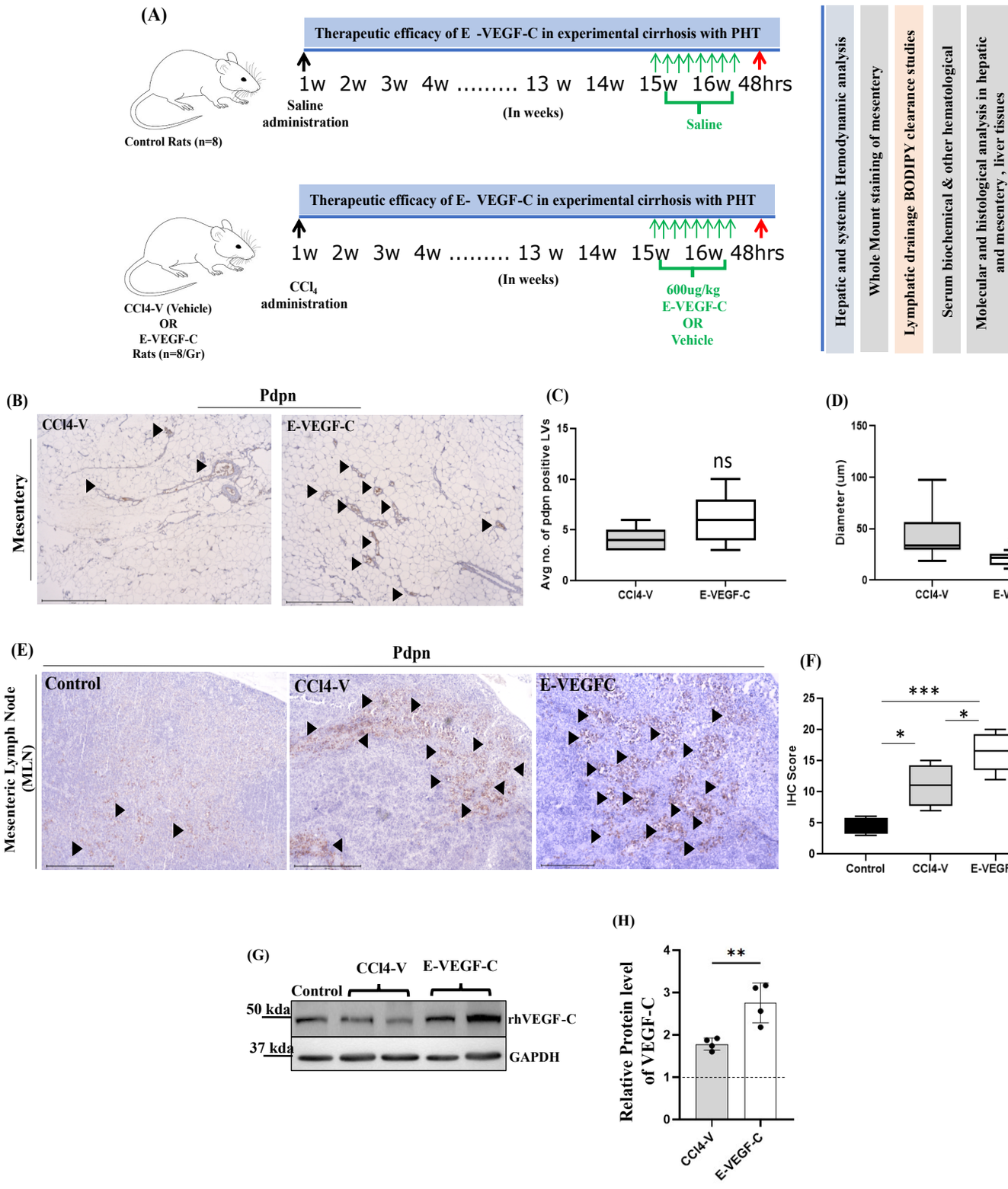
(A)
Therapeutic efficacy of E -VEGF-C in experimental cirrhosis with PHT
1w 2w 3w 4w ..... 13 w 14w 15w 16w 48hrs
Saline administration
(In weeks)
Saline
Control Rats (n=8)
Therapeutic efficacy of E- VEGF-C in experimental cirrhosis with PHT
1w 2w 3w 4w ..... 13 w 14w 15w 16w 48hrs
CCl4 administration
(In weeks)
600ug/kg E-VEGF-C OR Vehicle
CCl4-V (Vehicle) OR E-VEGF-C Rats (n=8/Gr)
Hepatic and systemic Hemodynamic analysis
Whole Mount staining of mesentery
Lymphatic drainage BODIPY clearance studies
Serum biochemical & other hematological
Molecular and histological analysis in hepatic and mesentery , liver tissues
(B)
Pdpn
Mesentery
CCl4-V
E-VEGF-C
(C)
Avg no. of pdpn positive LVs
ns
CCl4-V
E-VEGF-C
(D)
Diameter (um)
**
CCl4-V
E-VEGF-C
(E)
Pdpn
Mesenteric Lymph Node (MLN)
Control
CCl4-V
E-VEGFC
(F)
IHC Score
***
*
*
Control
CCl4-V
E-VEGFC
(G)
CCl4-V
E-VEGF-C
Control
50 kda
37 kda
rhVEGF-C
GAPDH
(H)
Relative Protein level of VEGF-C
**
CCl4-V
E-VEGF-C

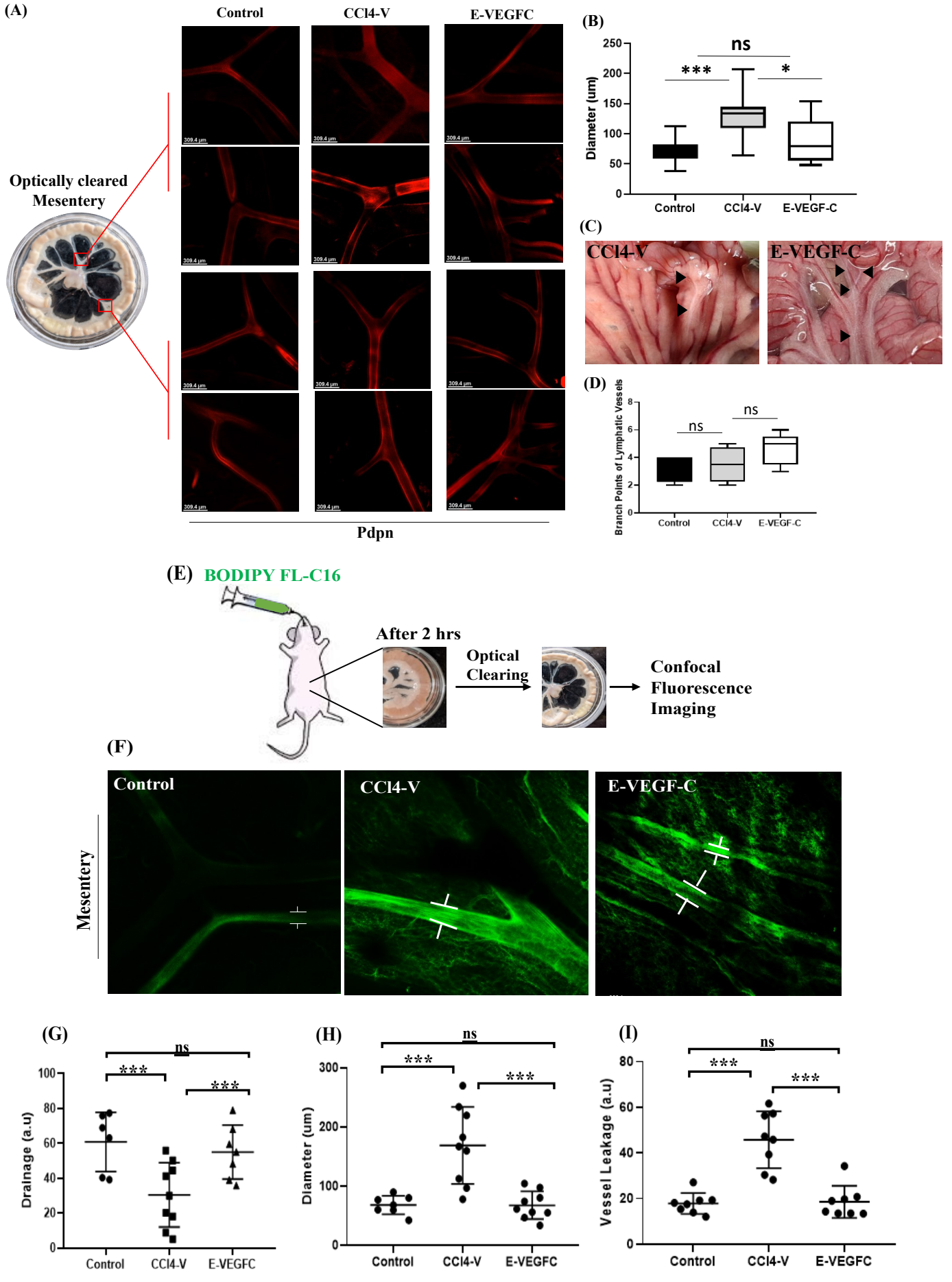
(A)
Control
CCl4-V
E-VEGFC
Optically cleared Mesentery
Pdpn
(B)
Diameter (um)
ns
***
*
Control
CCl4-V
E-VEGF-C
(C)
CCl4-V
E-VEGF-C
(D)
Branch Points of Lymphatic Vessels
ns
ns
Control
CCl4-V
E-VEGF-C
(E)
BODIPY FL-C16
After 2 hrs
Optical Clearing
Confocal Fluorescence Imaging
(F)
Mesentery
Control
CCl4-V
E-VEGF-C
(G)
Drainage (a.u)
ns
***
***
Control
CCl4-V
E-VEGFC
(H)
Diameter (um)
ns
***
***
Control
CCl4-V
E-VEGFC
(I)
Vessel Leakage (a.u)
ns
***
***
Control
CCl4-V
E-VEGFC

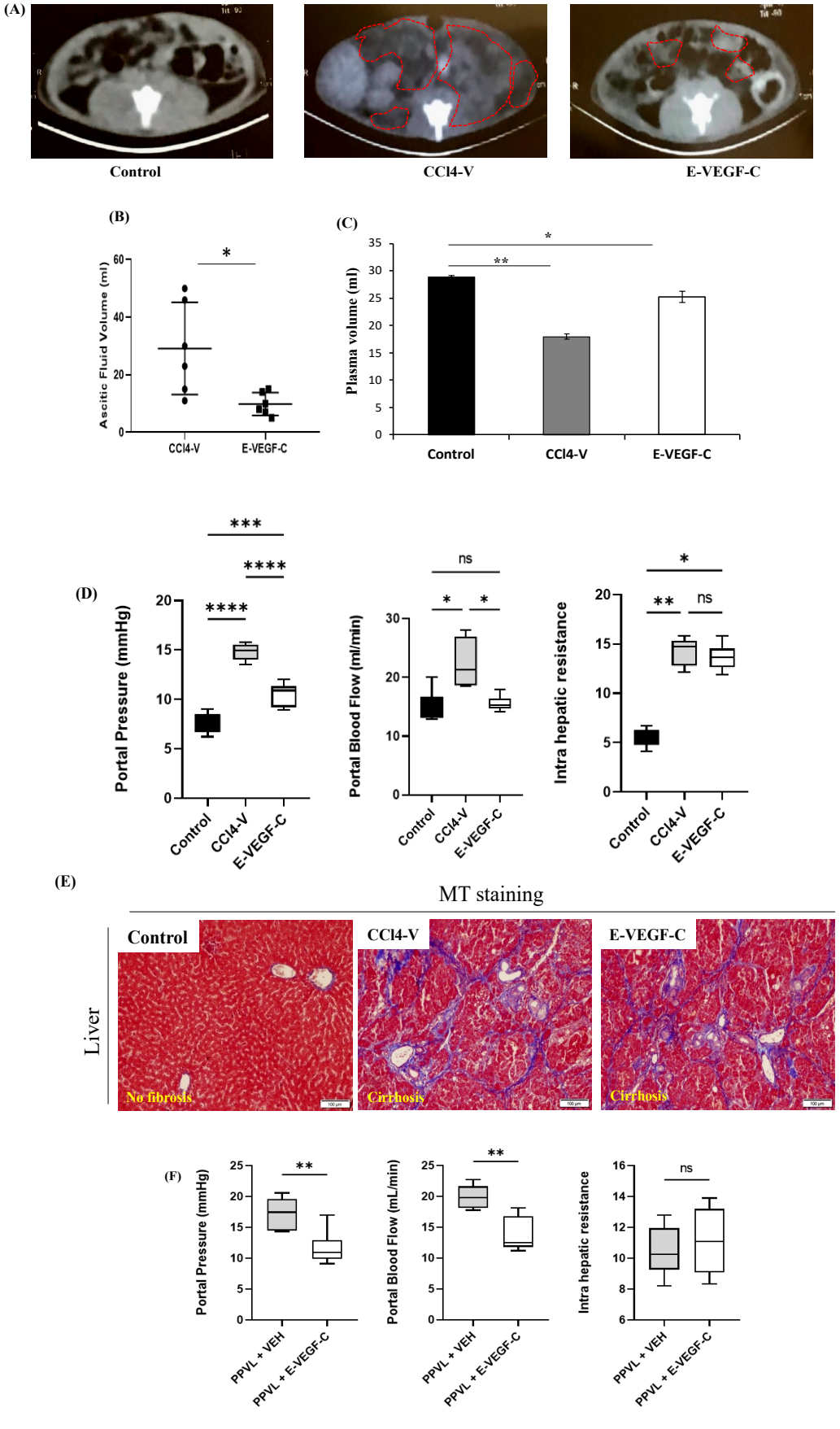
(A)
Control
CCl4-V
E-VEGF-C
(B)
Ascitic Fluid Volume (ml)
CCl4-V
E-VEGF-C
(C)
Plasma volume (ml)
Control
CCl4-V
E-VEGF-C
(D)
Portal Pressure (mmHg)
Portal Blood Flow (ml/min)
Intra hepatic resistance
Control
CCl4-V
E-VEGF-C
(E)
MT staining
Liver
Control
CCl4-V
E-VEGF-C
No fibrosis
Cirrhosis
Cirrhosis
(F)
Portal Pressure (mmHg)
Portal Blood Flow (mL/min)
Intra hepatic resistance
PPVL + VEH
PPVL + E-VEGF-C

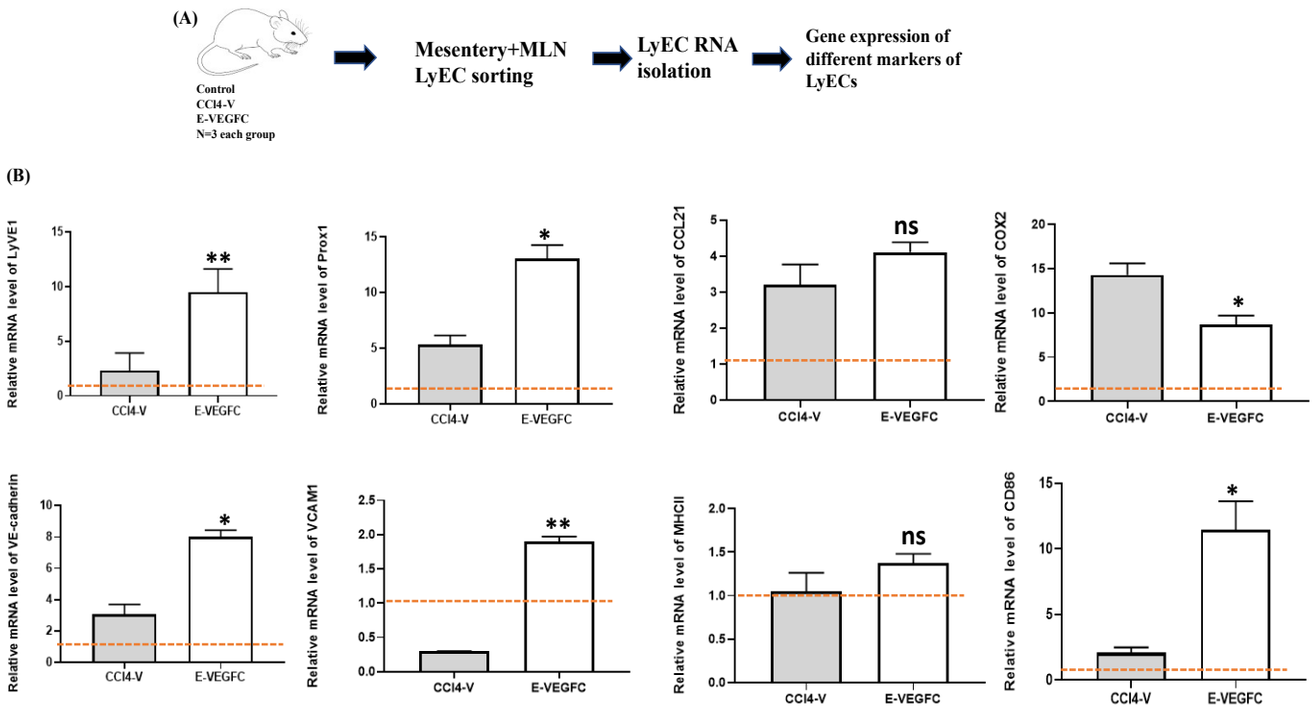
(A)
Control
CCl4-V
E-VEGFC
N=3 each group
Mesentery+MLN
LyEC sorting
LyEC RNA
isolation
Gene expression of
different markers of
LyECs
(B)
Relative mRNA level of LyVE1
Relative mRNA level of Prox1
Relative mRNA level of CCL21
Relative mRNA level of COX2
Relative mRNA level of VE-cadherin
Relative mRNA level of VCAM1
Relative mRNA level of MHCII
Relative mRNA level of CD86
CCl4-V
E-VEGFC
**
*
ns

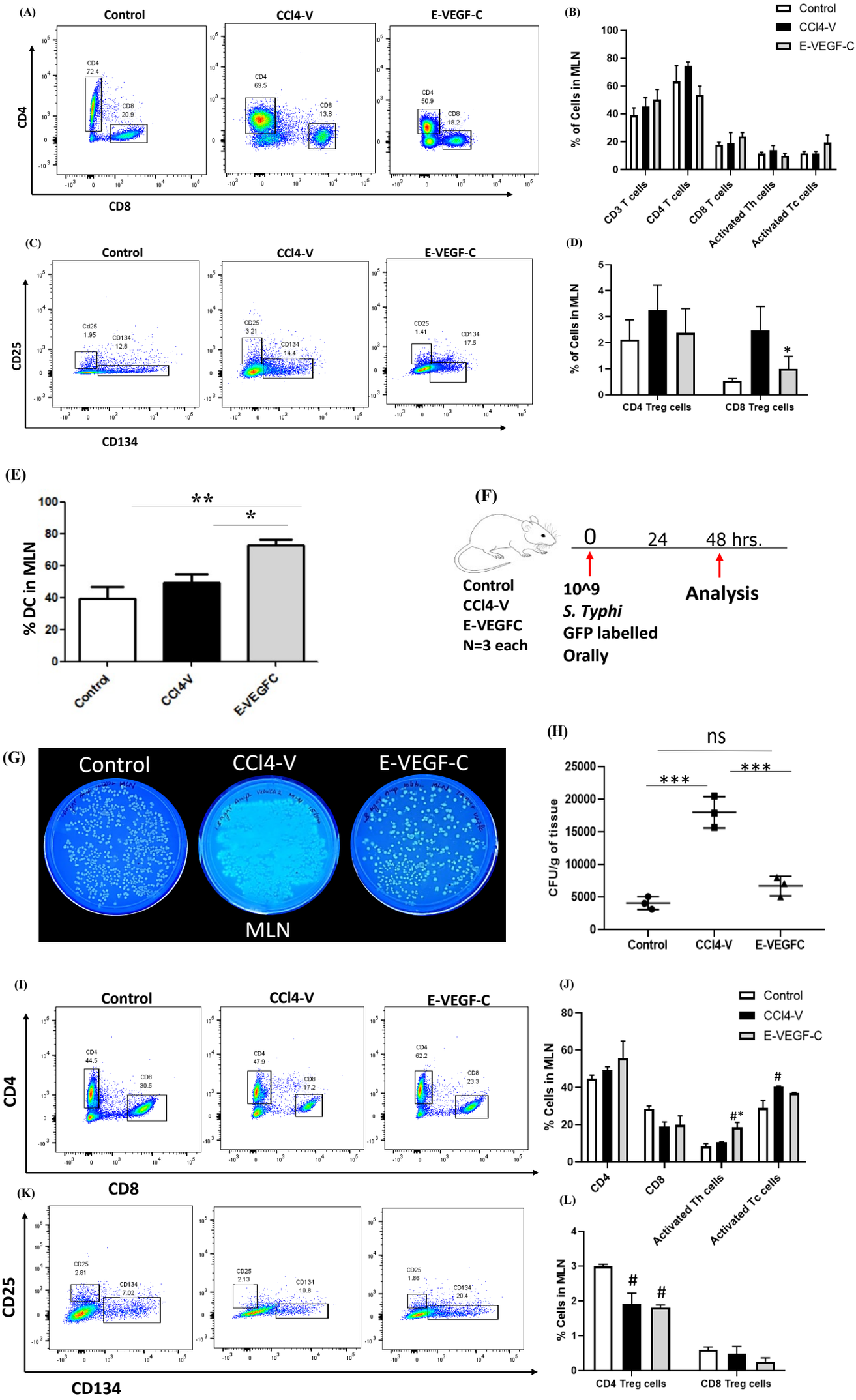
(A)
Control
CCl4-V
E-VEGF-C
CD4
CD8
CD4 72.4
CD8 20.9
CD4 69.5
CD8 13.8
CD4 50.9
CD8 18.2
(B)
Control
CCl4-V
E-VEGF-C
% of Cells in MLN
CD3 T cells
CD4 T cells
CD8 T cells
Activated Th cells
Activated Tc cells
(C)
Control
CCl4-V
E-VEGF-C
CD25
CD134
Cd25 1.95
CD134 12.8
CD25 3.21
CD134 14.4
CD25 1.41
CD134 17.5
(D)
% of Cells in MLN
CD4 Treg cells
CD8 Treg cells
(E)
% DC in MLN
Control
CCl4-V
E-VEGFC
(F)
0
24
48 hrs.
Control
CCl4-V
E-VEGFC
N=3 each
10^9
S. Typhi
GFP labelled
Orally
Analysis
(G)
Control
CCl4-V
E-VEGF-C
MLN
(H)
ns
CFU/g of tissue
Control
CCl4-V
E-VEGFC
(I)
Control
CCl4-V
E-VEGF-C
CD4
CD8
CD4 44.5
CD8 30.5
CD4 47.9
CD8 17.2
CD4 62.2
CD8 23.3
(J)
Control
CCl4-V
E-VEGF-C
% Cells in MLN
CD4
CD8
Activated Th cells
Activated Tc cells
(K)
CD25
CD134
CD25 2.81
CD134 7.02
CD25 2.13
CD134 10.8
CD25 1.86
CD134 20.4
(L)
% Cells in MLN
CD4 Treg cells
CD8 Treg cells

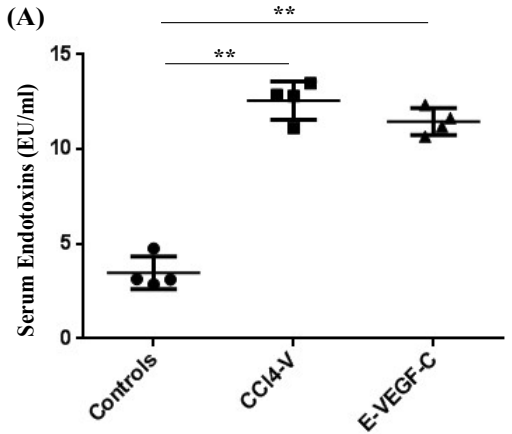
(A)
**
**
Serum Endotoxins (EU/ml)
15
10
5
0
Controls
CCl4-V
E-VEGF-C

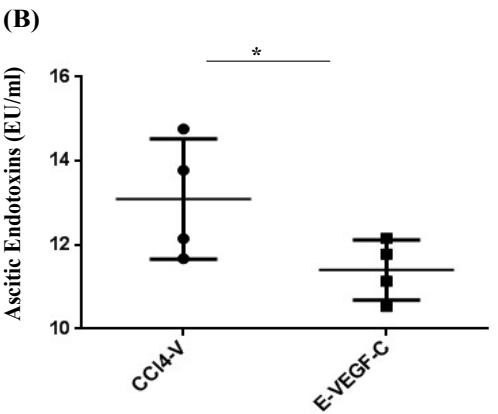
(B)
*
Ascitic Endotoxins (EU/ml)
16
14
12
10
CCl4-V
E-VEGF-C

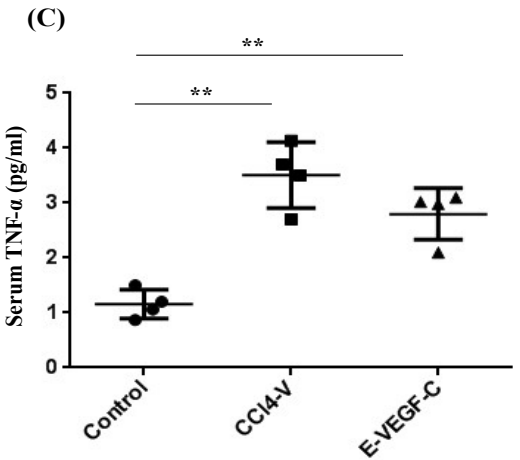
(C)
**
**
Serum TNF-α (pg/ml)
5
4
3
2
1
0
Control
CCl4-V
E-VEGF-C

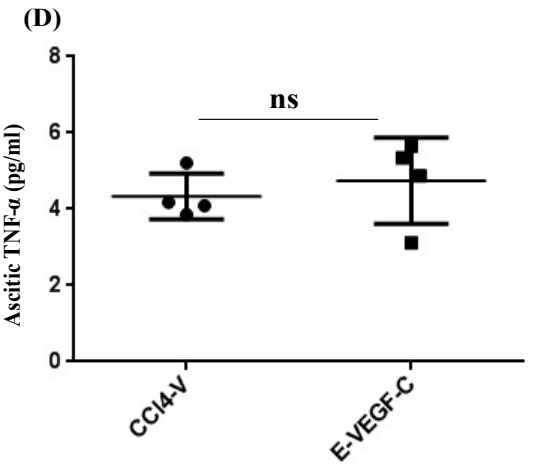
(D)
ns
Ascitic TNF-α (pg/ml)
8
6
4
2
0
CCl4-V
E-VEGF-C